Chemoreception and neuroplasticity in respiratory circuits

William H. Barnett[1], Ana P. Abdala[2], Julian F. R. Paton[2], Ilya A. Rybak[3], Daniel B. Zoccal[4], Yaroslav I. Molkov[1]

[1]Indiana University – Purdue University Indianapolis, IN

[2]School of Physiology and Pharmacology, University of Bristol, UK

[3]Drexel University College of Medicine, Philadelphia, PA

[4]São Paulo State University, Araraquara, Brazil

Corresponding author: Yaroslav I. Molkov, PhD
Department of Mathematical Sciences
Indiana University – Purdue University Indianapolis
402 N. Blackford St. LD270
Indianapolis, IN 46202
Email: ymolkov@iupui.edu

Keywords: respiration; obstructive sleep apnea; hypertension; chronic intermittent hypoxia; peripheral chemoreception; plasticity

Abstract

The respiratory central pattern generator must respond to chemosensory cues to maintain oxygen (O_2) and carbon dioxide (CO_2) homeostasis in the blood and tissues. To do this, sensorial cells located in the periphery and central nervous system monitor the arterial partial pressure of O_2 and CO_2 and initiate respiratory and autonomic reflex adjustments in conditions of hypoxia and hypercapnia. In conditions of chronic intermittent hypoxia (CIH), repeated peripheral chemoreceptor input mediated by the nucleus of the solitary tract induces plastic changes in respiratory circuits that alter baseline respiratory and sympathetic motor outputs and result in chemoreflex sensitization, active expiration, and arterial hypertension. Herein, we explored the hypothesis that the CIH-induced neuroplasticity primarily consists of increased excitability of pre-inspiratory/inspiratory neurons in the pre-Bötzinger complex. To evaluate this hypothesis and elucidate neural mechanisms for the emergence of active expiration and sympathetic overactivity in CIH-treated animals, we extended a previously developed computational model of the brainstem respiratory-sympathetic network to reproduce experimental data on peripheral and central chemoreflexes post-CIH. The model incorporated neuronal connections between the 2nd-order NTS neurons and peripheral chemoreceptors afferents, the respiratory pattern generator, and sympathetic neurons in the rostral ventrolateral medulla in order to capture key features of sympathetic and respiratory responses to peripheral chemoreflex stimulation. Our model identifies the potential neuronal groups recruited during peripheral chemoreflex stimulation that may be required for the development of inspiratory, expiratory and sympathetic reflex responses. Moreover, our model predicts that pre-inspiratory neurons in the pre-Bötzinger complex experience plasticity of channel expression due to excessive excitation during peripheral chemoreflex. Simulations also show that, due to positive interactions between pre-inspiratory neurons in the pre-Bötzinger complex and expiratory neurons in the retrotrapezoid nucleus, increased excitability of the former may lead to the emergence of the active expiratory pattern at normal CO_2 levels found after CIH exposure. We conclude that neuronal type specific neuroplasticity in the pre-Bötzinger complex induced by repetitive episodes of peripheral chemoreceptor activation by hypoxia may contribute to the development of sympathetic over-activity and hypertension.

Introduction

Hypertension is a highly prevalent public health problem that affects a large proportion of population worldwide (Kearney et al., 2005, Carey, 2013, Go et al., 2014). Accumulating evidence shows that reducing sympathetic nerve activity decreases blood pressure in hypertensive patients, especially in those who are resistant to pharmacologic antihypertensive treatment (Esler, 2009, Fisher and Paton, 2012), suggesting that sympathetic overactivity is a major contributor to the development and maintenance of hypertension. Moreover, experimental data indicate that increased activity of the sympathetic nervous system is pivotal for the development of high blood pressure in rodent models of hypertension (Simms et al., 2009, Malpas, 2010, Briant et al., 2015). This scenario of hypertension and sympathetic overactivity is observed in obstructive sleep apnea (OSA) patients (Narkiewicz et al., 1998). OSA is a condition characterized by recurrent upper airway collapses during sleep and affects approximately 20% of adult population in USA (Konecny and Somers, 2011). Untreated OSA has cumulative effects on the cardiovascular system, leading to augmented baseline sympathetic activity and arterial hypertension that can be refractory to pharmacological therapies (Williams et al., 2010, Pedrosa et al., 2011). Studies estimate that 50–56% of individuals with OSA are hypertensive (Dudenbostel and Calhoun, 2011).

Clinical and experimental evidence suggests that chronic exposure to intermittent hypoxia (CIH) is a main factor leading to cardiovascular dysfunction in OSA patients (Fletcher, 2001, Caples et al., 2005). In rats, CIH promotes hypertension linked to elevated baseline sympathetic vasomotor tone and higher noradrenaline plasma levels (Braga et al., 2006, Zoccal et al., 2007, Zoccal et al., 2008, Zoccal et al., 2009) highlighting a relationship among CIH, sympathetic overactivity and hypertension. Importantly, the high levels of sympathetic activity of CIH rats were associated with strengthened coupling between respiratory and sympathetic networks. Indeed, we originally reported (Zoccal et al., 2008) that CIH exposure promotes an increase in sympathetic activity during the expiratory phase, specifically during the late part of expiration (late-E). These additional expiratory bursts in sympathetic activity of CIH rats were coupled to the late-E bursts emerging in the abdominal expiratory motor output. Moreover, the late-E activity was present at rest in eucapnia in CIH-treated animals but

never in untreated controls, and was eliminated by a reduction of CO_2 content in the perfusate (Molkov et al., 2011). The involvement of respiratory-sympathetic interactions in the development of hypertension in CIH rats is further supported by recent findings that late-E modulation in the pre-sympathetic neurons of rostral ventrolateral medulla (RVLM) depends on synaptic inputs from bulbar respiratory neurons rather than on changes in their intrinsic properties (Moraes et al., 2013, Moraes et al., 2014). All together these data indicate that CIH-induced sympathetic overactivity is linked to the transition of expiration from a passive to an active process at rest. These findings represent novel and unexplored aspects of central mechanisms underpinning arterial hypertension in CIH rats (Moraes et al., 2012b).

The development of arterial hypertension in rats exposed to CIH is fully prevented by previous ablation of carotid body peripheral chemoreceptors (Fletcher et al., 1992), indicating that the plasticity in the neural circuitries of the peripheral chemoreflex, elicited by repeated stimulation during CIH (Moraes et al., 2015), may underpin the development of the observed respiratory and sympathetic changes. Therefore, it is important to understand the neural pathways engaged during peripheral chemoreceptor stimulation in order to identify potential neural mechanisms triggering active expiration and sympathetic overactivity in CIH rats. Here, we develop the hypothesis that central plasticity accounts for the facilitation of sympathetic and respiratory response to peripheral chemoreflex in CIH conditioned rats. Accordingly, the objectives of this study were (i) to model the neural pathways required for the adjustments in the respiratory and sympathetic motor outputs during peripheral chemoreflex activation, (ii) to understand the functional implications of their repetitive activation during CIH conditioning, and (iii) to shed light on where within the network the origin of neuronal plasticity occurs that is responsible for the sustained active expiration and sympathoactivation following CIH exposure.

Methods

In the present study, we combined recent published studies (Braga et al., 2006, Zoccal et al., 2008, Molkov et al., 2011, Moraes et al., 2012a, McBryde et al., 2013,

Moraes et al., 2014) and new experimental data obtained in the *in situ* arterially perfused preparation of decerebrate rats, as described in details below.

Experimental data

Animals and ethical approval

Experiments were performed on male Holtzman rats, weighing 70-90 g, obtained from the Animal Care Unit of the São Paulo State University, Araraquara, and kept at 22±1 °C on a 12-h light/dark cycle (lights on 06:00 – lights off 18:00), with access to food and water *ad libitum*. All experimental approaches followed the Guide for the Care and Use of Laboratory Animals published by the US National Institutes of Health (NIH publication No. 85-23 revised 1996) and by the Brazilian National Council for Animal Experimentation Control (CONCEA), and was approved by the Local Ethical Committee in Animal Experimentation (protocol 18/2014).

Chronic intermittent hypoxia (CIH)

The rats were exposed to CIH as previously described (Zoccal et al., 2008). Briefly, the animals were housed in collective cages (maximum of 5 animals per cage) and maintained inside chambers equipped with gas injectors as well as sensors of O_2, CO_2, humidity and temperature, at controlled conditions of temperature (22±1°C) and humidity (55±10%). The CIH protocol consisted of 5 minutes of normoxia (FiO_2 of 20.8%) followed by 4 minutes of pure N_2 injection into the chamber in order to reduce the fraction of inspired O_2 (FiO_2) to 6%, remaining at this level for 40 seconds. After this hypoxic period, pure O_2 was injected to return the FiO_2 back to 20.8%. This 9-minute cycle was repeated 8 hours a day (from 9:30 am to 5:30 pm) for 10 days. During the remaining 16 hours, the animals were maintained at a FiO_2 of 20.8%. The injections of N_2 and O_2 (White Martins, São Carlos, Brazil) were regulated by a solenoid valve system whose opening-closing control was performed by a computerized system (Oxycycler, Biospherix, USA). In an identical chamber in the same room, the control group was exposed to a FiO_2 of 20.8% 24 hours a day for 10 days. The control rats were also exposed to a similar valve noise due to the frequent injection of O_2 to maintain the FiO_2 at

20.8%. In both CIH and control chambers, the gas injections were performed at the upper level of the chamber in order to avoid direct jets of gas impacting on the animals, which could cause stress.

In situ arterially perfused preparation of decerebrate rats

Arterially perfused *in situ* preparations (Paton, 1996) of control and CIH rats were surgically prepared, as previously described (Zoccal et al., 2008). The rats were deeply anesthetized with halothane (AstraZeneca, Cotia, SP, Brazil) until loss of paw withdrawal reflex, transected caudal to the diaphragm, submerged in a chilled Ringer solution (in mM: NaCl, 125; $NaHCO_3$, 24; KCl, 3; $CaCl_2$, 2.5; $MgSO_4$, 1.25; KH_2PO_4, 1.25; dextrose, 10) and decerebrated at the precollicular level. Lungs were removed. Preparations were then transferred to a recording chamber, the descending aorta was cannulated and perfused retrogradely with Ringer solution containing 1.25 % Polyethylene glycol (an oncotic agent, Sigma, St Louis, USA) and a neuromuscular blocker (vecuronium bromide, 3-4 $\mu g.mL^{-1}$, Cristália Produtos Químicos Farmacêuticos Ltda., São Paulo, Brazil), using a roller pump (Watson-Marlow 502s, Falmouth, Cornwall, UK) via a double-lumen cannula. The perfusion pressure was maintained in the range of 50–70 mmHg by adjusting the flow rate to 21- 25 $ml.min^{-1}$ and by adding vasopressin to the perfusate (0.6 – 1.2 nM, Sigma, St. Louis, MO, USA). The perfusate was gassed continuously with 5% CO_2-95% O_2, warmed to 31–32°C and filtered using a nylon mesh (pore size: 25 μm, Millipore, Billirica, MA, USA). Sympathetic and respiratory nerves were isolated and their activity recorded simultaneously using bipolar glass suction electrodes held in micromanipulators (Narishige, Tokyo, Japan). Left phrenic nerve (PN) discharges were recorded from its central end and its rhythmic ramping activity was used to monitor preparation viability. Left cervical vagus (cVN) and hypoglossal nerves (HN) as well as right thoracic/lumbar abdominal nerves (AbN; T13-L1) were isolated, cut distally and their central activity recorded. Thoracic sympathetic activity was recorded from the left sympathetic chain (tSN) at T8–T12 level. All the signals were amplified, band-pass filtered (0.1–3 kHz; P511, Grass Technologies, Middleton, USA) and acquired in an A/D converter (CED micro 1401, Cambridge Electronic Design, CED, Cambridge, UK) to a computer using Spike 2 software (5 KHz, CED, Cambridge, UK). At the end of

the experiments, the perfusion pump was turned off to determine the electrical noise (after the death of the preparations).

All analyses were carried out on rectified and integrated signals (time constant of 50 ms) and performed off-line using Spike 2 software (CED, Cambridge, UK) after noise subtraction. PN burst frequency was determined from the time interval between consecutive integrated phrenic peak bursts and expressed in bursts per minute (bpm). tSN activity was measured as the mean values (in μV) of integrated signals. The changes in the PN burst frequency and tSN in response to peripheral chemoreflex activation were expressed as percentage values in relation to basal values prior to the stimulus.

Peripheral chemoreflex activation

Peripheral chemoreceptors were stimulated in the *in situ* preparations by injections of potassium cyanide (KCN 0.05%, 50 μl) into the descending aorta via the perfusion cannula as described previously (Costa-Silva et al., 2010). Stimulation of the peripheral chemoreflex receptors by KCN produced consistent autonomic and respiratory responses, which present low variability within and among the experiments.

Statistical analyses

The data were expressed as mean ± standard error of mean (SEM). Before analysis, data distribution was tested using the Shapiro–Wilk normality test. The sympathoexcitatory and tachypneic responses to peripheral chemoreceptor activation in control and CIH rats were compared using, unpaired Student's t-test or two-way ANOVA for repeated measurements followed by Newman-Keuls post-test, respectively. The analysis was carried out using GraphPad Prism software (version 5, La Jolla, CA, USA) and differences were considered significant at $P < 0.05$.

Modeling and simulations

The model presented here is based on a previous model of central chemoreceptor sensitization from (Molkov et al., 2011, Molkov et al., 2014b), which in turn combined a model describing the origin of abdominal late-E activity (Molkov et al., 2010) and a

model describing sympathy-respiratory coupling in the context of the baroreflex (Baekey et al., 2010). All of these models descend from the model described by Rybak et al. (2007) and Smith et al. (2007), which explain the change in respiratory patterns due to successive pontine and medullary transections performed in rats. Most neuronal populations were composed of single-compartment Hodgkin-Huxley style neuronal models. Each population contained 20 or 50 neurons. Neurons in postsynaptic populations each received input from every neuron in the presynaptic population or the appropriate drive element. The output of certain populations, including motoneurons, was obtained by integrating excitatory synaptic input. Heterogeneity of model parameters and initial conditions (such as membrane potential, calcium concentration, and gating variables) were set by random distributions. Parameters for synaptic weights including changes relative to Molkov et al. (2011) can be found in Table 1.

Simulations were performed using the NSM simulation package version 3.0 developed at Drexel University by S. Markin, I. Rybak, and N. Shevtsova and ported for parallel computing on high-performance clusters using OpenMPI by Y. Molkov. Numerical solutions to ordinary differential equations were computed using the exponential Euler method for integration with a step of 0.1 ms.

Results

Peripheral chemoreflex, respiratory and sympathetic adjustments and exposure to chronic intermittent hypoxia: experimental evidence

Effects of CIH on CO_2 threshold for apnea and active expiration in rats in situ

We previously demonstrated (Molkov et al., 2011) that rats exposed to chronic intermittent hypoxia exhibit changes in excitability within the respiratory network. This was verified by the evaluation of the respiratory responses to varying levels of CO_2. Figure 1 shows the AbN and PN motor patterns in *in situ* preparations of control rats (upper traces) and in rats after CIH conditioning (lower traces) at different CO_2 contents in the perfusate: normocapnia (5% CO_2, middle traces); hypercapnia (7% and 10% CO_2, right traces) and hypocapnia (1% and 3% CO_2, left traces). As it is evident from the

figure, in normocapnia control rats exhibited a passive expiratory pattern, as only PN activity showed rhythmic discharges of inspiratory activity, and AbN remained fairly quiescent. With progressive increase in CO_2 large amplitude discharges appeared in the AbN activity of control rats at the late-E phase of the respiratory cycle signifying a transition to active expiration. In CIH-conditioned rats, AbN late-E discharges were present during normocapnia. Lowering CO_2 content to 3% abolished these discharges. So, the CO_2 threshold for transition to active expiration was between 5% and 7% for naïve animals, and between 3% and 5% for the CIH conditioned rats.

As CO_2 level decreased from 3% to 1% the PN rhythmic activity ceased in naïve animals but not in rats exposed to CIH (see first column in Fig. 1, which depicts representative traces from one control rat and one CIH conditioned rat). These results imply that the CO_2 apneic threshold was between 1% and 3% CO_2 in the control group, and below 1% in the CIH animals. Accordingly, both thresholds for apnea and for the transition to active expiration are approximately 2% CO_2, lower in CIH conditioned animals as compared to naïve rats. All data quantification and analyses are presented in details in(Molkov et al., 2011).

Respiratory and sympathetic adjustments elicited by peripheral chemoreflex activation

Previous studies have demonstrated the changes in the pattern of PN, tSN and AbN activities in response peripheral chemoreflex activation (Dick et al., 2004, Moraes et al., 2012a). Herein, we extended this characterization and also evaluated the changes in cVN and HN activities. Transient stimulation of CB peripheral chemoreceptors of control *in situ* preparations with KCN (n=7) had a profound effect on activity patterns in all motor outputs that lasted 10-15s (see Fig. 2 for typical responses). There was an approximately two-fold increase in respiratory frequency (ΔPN frequency: 114±18%, from 22±6 to 46±6 bpm, $P<0.05$; Fig. 2C) accompanied by augmented post-inspiratory amplitude recorded from the cVN (ΔcVN: 68±5%, $P<0.05$, Fig. 2C) and an abrupt rather than decrementing ending as seen during baseline activity. Abdominal, hypoglossal and sympathetic nerve activities also increased mainly during the post-I period (ΔAbN: 105±34 %, ΔHN: 149±25 %, ΔtSN: 94±5 %, $P<0.05$, Fig. 2C). Importantly, at the end of the stimulus these strong post-I discharges disappeared from all

nerves simultaneously suggesting that they may had a common origin. In addition, the AbN and HN exhibited late-E discharges during stimulation that strongly resembles hypercapnia-evoked late-E activity. Similar late-E related discharges were also seen in the sympathetic outflow.

It was previously suggested that the source of late-E AbN activity activated by hypercapnia was in the RTN/pFRG (Janczewski and Feldman, 2006, Abdala et al., 2009, Molkov et al., 2010). To understand if the AbN modulation induced by peripheral chemoreflex originates from the same location, Moraes et al. (2012a) suppressed the RTN activity by muscimol ($GABA_A$ receptor agonist) before stimulating peripheral chemoreceptors by KCN. Interestingly, late-E discharges disappeared from both abdominal and sympathetic nerves without affecting the post-I responses. This observation suggests that post-I and late-E activities in AbN and tSN during peripheral chemoreflex have different origins. Late-E activity most probably has the same source as observed during hypercapnia originating from the RTN, whereas the source of post-I activity is located elsewhere.

Exaggerated respiratory and sympathetic chemoreflex responses after CIH exposure

Typical recordings of PN, tSN, AbN and cVN activities of control and CIH rats, illustrating the pattern of changes in response to peripheral chemoreflex activation, are shown in Fig. 3A and B. Consistent with previous observations (Braga et al., 2006), we verified that *in situ* preparations of CIH rats (n=8) exhibited amplified sympathoexcitatory responses to peripheral chemoreflex stimulation (128±8 vs 94±5%, $P < 0.05$, Fig. 3C) in comparison to the control group (n=7). The enhanced sympathetic chemoreflex response in CIH rats also showed augmented respiratory modulation, with bursts occurring preferentially during the post-inspiratory phase. In relation to the PN frequency, the analysis of percentage changes respective to basal values indicated that CIH and control groups presented a similar increase in the magnitude of PN frequency (80±21 vs 114±18%, 2s after stimulation, respectively). However, the PN frequency remained elevated at 4 (144±36 vs 77±12%, $P < 0.01$) and 6s (151±36 vs 66±13%, $P < 0.001$) after the stimulation of peripheral chemoreceptors in CIH rats, indicating prolongation of tachypnea (Fig. 3D). With respect to AbN chemoreflex response, the

magnitude of increase was similar in both groups (104±21 vs 105±34%, Fig. 3E). However, a different pattern of AbN response is observed in CIH in relation to control rats. In control rats, the relative increase in AbN expiratory activity occurs during the post-inspiration (55±2% of the response) and late expiration (45±2% of the response), with prevalence in the former ($P<0.05$, Fig. 3F). In the CIH group, however, the evoked AbN response is shifted towards the late expiratory phase (late expiration: 65±2% vs post-inspiration: 35±2%, $P < 0.001$, Fig. 3F),. The magnitude of increase in cVN in response to KCN was similar between CIH and control groups (75±8 vs 68±5 %, respectively, Fig. 3G). Together, these data supports the notion that the processing of sympathetic, inspiratory and late-expiratory responses to peripheral chemoreflex is facilitated in rats exposed to CIH.

Pre-I/I neurons in spontaneously hypertensive rats

In a different animal model of neurogenic hypertension, the spontaneously hypertensive rat (SHR), Moraes et al. (2014) demonstrated that intrinsically bursting neurons in the pre-BötC were found to have altered electrophysiological properties. Specifically, the authors showed that pre-BötC pre-inspiratory neurons are more excitable due to significantly lower conductance of the leak current. Interestingly, SHR and CIH rat models of hypertension share many common features: 1) strengthened respiratory-sympathetic coupling are suggested to be involved in the development/maintenance of arterial hypertension (Zoccal et al., 2008, Moraes et al., 2014); 2) the carotid body chemoreceptors play a pivotal role for the development of hypertension (Fletcher et al., 1992, Abdala et al., 2012); 3) the sympathetic response to peripheral chemoreceptors are amplified in SHR and CIH rats (Braga et al., 2006, Simms et al., 2009, Tan et al., 2010, Moraes et al., 2014), suggesting a sensitization of processing of peripheral chemoreceptor inputs; 4) presence of a late-expiratory component in the AbN, in the cervical sympathetic and in the pre-sympathetic RVLM neuronal activity at normal (5%) CO_2 levels strongly resembling the respiratory pattern of control (Wistar) animals at 7% CO_2 (Zoccal et al., 2008, Moraes et al., 2013, Moraes et al., 2014); and 5) a lower apneic threshold compared to Wistar rats (Moraes et al., 2014) (Molkov et al., 2011). Based on these similarities, we hypothesize that CIH-conditioned animals have altered baseline

respiratory patterns due to increased excitability of pre-I/I population in pre-BötC because of the reduced leak conductance of these neurons (Moraes et al., 2014, 2015). We tested this hypothesis using computational modeling.

Effects of peripheral chemoreceptor activation on the brainstem respiratory and sympathetic networks: insights from computational modeling

Model description

The main objective of the modeling part of our study was to provide mechanistic interpretation of the processes involved in peripheral chemoreflex modulation of the respiratory and pre-sympathetic networks. This included: (1) an increase in respiratory frequency; (2) the appearance of post-I activity in the HN, AbN, and tSN and an augmentation of post-I activity amplitude in the cVN; (3) the appearance of late-E activity in the HN, AbN, and tSN; and (4) an increase in respiratory-independent activity of tSN.

The model included a population of 2nd-order cells in the NTS receiving peripheral chemoreceptor inputs and their efferent projection to ventromedullary compartments. The schematic of the extended model is shown in Fig. 4.

We extended the model to include new neuronal populations that mediate the peripheral chemoreflex. During peripheral chemoreflex, input from the carotid body (CB) was represented by a constant drive to the 2nd-order NTS neurons. This population of simple spiking neurons distributed excitatory projections to the respiratory and sympathetic circuits. To account for the increase in respiratory frequency, which should primarily occur through shortening of the E2 phase, we implemented direct excitation from the 2nd-order NTS neurons to the early-I (1) and pre-I/I populations of the pre-BötC. The pre-I/I population is the primary excitatory population contributing to the initiation of inspiration.

To account for the post-I activity in motoneuron output, we introduced another post-I population (bulbo-spinal cVRG). This population receives tonic excitation from the 2nd-order NTS neurons during peripheral chemoreflex. In addition, the activity of this population is modulated by the respiratory CPG; inhibition from aug-E and early-I (2)

shape its output to allow only post-I activity. This population receives tonic excitation from 2nd-order chemoreceptive neurons in the NTS. Activation of this population during inspiration is prevented by inhibition from early-I (2); activation of this population during E2 is suppressed by inhibition from aug-E. Thus, activation of and excitation from the 2nd-order chemoreceptive NTS neurons translate to post-I activity in the cVRG. This post-I (cVRG) population is responsible for post-I activity in the HN, AbN, and tSN and augments the post-I component in the cVN.

In our previous model, we described how CO_2-sensitive drive from the RTN mediated the central chemoreflex in respiratory circuits (Molkov et al., 2010, Molkov et al., 2011). Increased drive from the RTN could drive the pFRG late-E population to threshold, and in this way, the central chemoreflex induces the onset of bursting activity in the pFRG, which is observed as late-E activity in the AbN. In the extended model, a CO_2-sensitive drive excites two distinct neuronal populations in the RTN (RTN-late-E and RTN-cpg) (see Fig. 4). One of these populations—the RTN-cpg—also received input from 2nd-order NTS chemoreceptive neurons. The dynamics of individual neurons in these two RTN populations were not modeled; rather, we directly simulated the firing rate of the population. The RTN-cpg population projected to: pre-I/I (pre-BötC), early-I (1) (pre-BötC), post-I (BötC), and late-E (pFRG). The RTN-late-E population projected only to the late-E population of the pFRG. Therefore, the pFRG late-E population receives excitatory projections from both peripheral chemoreflex sensitive and peripheral chemoreflex insensitive central chemoreceptive populations in the RTN. The CO_2-dependence of RTN-cpg and RTN-late-E is the same and mediates the central chemoreflex in a similar fashion to the direct CO_2-sensitive drive in Molkov et al. (2011). Progressive hypercapnia and hypocapnia were modeled by changing the magnitude of the CO_2 sensitive drive to RTN-cpg and RTN-late-E.

Since stimulation of the peripheral chemoreceptors can initiate late-E activity in the AbN, which is RTN-dependent (Moraes et al., 2012a), we extended the model to include excitation from 2nd-order NTS peripheral chemoreceptive neurons to augment excitatory drive from the RTN to the CPG. We implemented a direct projection from the 2nd-order NTS chemoreceptive neurons to the RTN-cpg population. The RTN-cpg population distributes both central and peripheral chemosensory drive to the respiratory

circuits. Notice that the RTN-late-E population does not receive excitation from the 2nd-order NTS chemoreceptive neurons, so this component of excitatory input to the pFRG late-E population is dependent on the central chemoreflex but independent of the peripheral chemoreflex.

The model by Baekey et al. (2010) described the baroreflex circuits, including 2nd-order baroreceptive NTS neurons and the pre-sympathetic circuits in the ventrolateral medulla. In that model, 2nd-order baroreceptive NTS neurons directly excited the CVLM, which inhibited RVLM to provide sympathoinhibition. Here, we implement a parallel pathway where 2nd-order peripheral chemoreceptive NTS neurons project directly to the RVLM in order to mediate sympathoexcitation during peripheral chemoreflex for which there is experimental evidence (Aicher et al., 1996, Koshiya and Guyenet, 1996).

As mentioned above, hypercapnia induces late-E activity in the AbN. CIH rats experience a hypocapnic shift in the threshold for emergence of this late-E activity (Abdala et al., 2009, Molkov et al., 2010, Molkov et al., 2011) (Fig. 1). On the other hand, experimental evidence in SHR suggests that the pre-I/I population in the pre-BötC becomes more excitable via a decrease in leak conductance (Moraes et al., 2014). We used this evidence to formulate the hypothesis that repetitive activation of peripheral and, hence, central chemoreceptors during CIH (see emphasized excitatory projections in Fig. 4) conditioning induces plasticity in this population as recently proposed (Moraes et al., 2015, Zoccal, 2015); specifically, we modelled the respiratory plasticity evoked by CIH as a decrease in the leak conductance of the pre-I/I population. The average leak conductance of these neurons was decreased from 2.9 nS in the control model to 2.3 nS in the CIH model. In order for the increase in excitability of the pre-I/I population to contribute to the excitability of the late-E (pFRG) population, we implemented a direct excitatory projection from pre-I/I (pre-BötC) to late-E (pFRG). The relative increase of the sympathoexcitatory response to peripheral chemoreceptor activation was implemented by a change in the chemosensory drive to 2nd-order peripheral chemoreceptive NTS neurons (see Table 1).

Simulation of peripheral chemoreceptor activation in naïve rats

The extended model was used to investigate the effects of peripheral chemoreceptors activation on the respiratory-sympathetic networks. Fig. 5A and Fig. 6A depict the activity of the respiratory circuits during normal conditions and during activation of peripheral chemoreceptors. A square pulse of excitatory drive to the 2nd-order NTS chemoreceptive neurons elicited an increase in network frequency which was based on the additional excitation to pre-I/I and early-I (1) neurons that overcame inhibition from the inhibitory populations in the BötC and initiate inspiration. Hence, the expiratory phase decreased in duration. Specifically, the duration of bursts in the aug-E and post-I populations of the BötC decreased (Fig. 6A). However, the duration of inspiration (Fig. 5A) and the burst duration of early-I (1) (Fig. 6A) did not change substantially. After peripheral chemoreceptor stimulation, the model captured the appearance of post-I activity in the HN, AbN, and tSN and increased post-I activity in the cVN that are prevalent in experimental recordings (Fig. 7). In the model, this activity was driven by the post-I (cVRG) population; it was silent without input from 2nd-order NTS chemoreceptive neurons, and received respiratory modulation in the form of inhibition from BötC aug-E and strong inhibition from pre-BötC early-I (1) (see Fig. 4). This inhibition occurred in the I-phase and E2-phase of respiration (Fig. 6A).

We propose that 2nd-order NTS chemoreceptive neurons project directly to central chemosensory populations of the RTN. During peripheral chemoreceptor activation, the CO_2 sensitive drive from RTN-cpg to the respiratory circuits is augmented. Hence, the pathway for stimulation of the late-E (pFRG) population becomes active (Fig. 6A). The model captured the appearance of late-E activity in the HN, AbN, and tSN that is prevalent in experimental recordings. The increase in drive to the pFRG was sufficient to induce periodic bursts of activity immediately preceding each inspiratory burst (Fig. 7). Tonic and respiratory-modulated activity in tSN during peripheral chemoreceptor activation increased due to converging direct and indirect excitatory pathways to RVLM. RVLM possessed a strong post-I component due to excitation from the post-I population in cVRG and a late-E component originating from the pFRG (Fig. 7).

Simulation of transient activation of peripheral chemoreceptors in naïve rats with RTN suppressed

Evidence suggests that late-E activity in the AbN during hypercapnia is dependent on an excitatory drive from the RTN (Molkov et al., 2010, Moraes et al., 2012a). Moreover, late-E activity in the AbN is abolished upon suppression of the RTN (Moraes et al., 2012a). Here, we reproduce experimental results of RTN suppression in the model. Fig. 5B and Fig. 6B depict activation of peripheral chemoreceptors with the RTN suppressed. To simulate the effects of muscimol injected in the RTN, we inhibited the central chemosensory populations in the RTN and the late-E pacemaker in pFRG. This manipulation was mimicked by reducing the CO_2 sensitive drive to RTN-cpg and RTN-late-E from 1.08 nS to 0.84 nS. Input from 2nd-order NTS peripheral chemoreceptive neurons to the central chemosensory complex in the RTN was not able to overcome inhibition by muscimol and activate the late-E population. The activation of the post-I population in the cVRG and the projections from the 2nd-order NTS chemoreceptive neurons into the respiratory CPG and pre-sympathetic groups was unaffected by suppression of the RTN (Fig. 5B and Fig. 6B). Due to the inhibition of the RTN, the late-E population in the pFRG remained silent during peripheral chemoreceptor activation (Fig. 6B), and hence, no late-E activity appeared in the AbN and tSN motor outputs (Fig. 5B). Decrease in drive to the RTN also reduces drive distributed to the CPG; RTN suppression induces a reduction in the baseline frequency of the respiratory rhythm.

Simulation of transient activation of peripheral chemoreceptors in CIH rats

The main difference in the effect of peripheral chemoreceptors in CIH compared to naïve rats is a substantial increase in sympatho-excitation (Braga et al., 2006) (Fig. 3). The tonic component of sympatho-excitation is mediated by a direct projection from 2nd-order NTS chemoreceptive neurons to the pre-sympathetic RVLM. Activation of this chemosensory drive leads to a tonic component to the sympathetic outflow during peripheral chemoreceptor activation by means of this direct projection to RVLM (Fig. 8A). To accommodate an increase in sympatho-excitation in CIH compared to the control model, we increased the amplitude of the peripheral chemoreceptor input by a factor of approximately 2. During peripheral chemoreceptor activation, the firing frequency of 2^{nd}-order NTS chemoreceptive neurons is greater in the CIH model than in the control model. As such, the efficacy of the excitatory projection to RVLM is greater,

which causes greater sympathetic outflow in the CIH model upon activation of the peripheral chemoreceptors (Fig. 8B). These effects of increased chemosensory drive in the CIH model are only visible during activation of the peripheral chemoreceptors. sensors.

Simulation of progressive hypercapnia and hypocapnia in the naïve model and the CIH model

A hallmark of CIH in the respiratory circuits is a hypocapnic shift in the threshold for the emergence of self-sustained rhythmic respiratory activity (apneic threshold) and a hypocapnic shift in the threshold for the emergence of active expiration. Previously, we described these changes in terms of direct sensitization of the RTN to the partial pressure of CO_2 in the blood (Molkov et al., 2011, Rybak et al., 2012, Molkov et al., 2014b). The previous model does not describe the mechanism by which CIH induces plasticity in the respiratory CPG. As described above, the pre-I/I population in the pre-BötC of SHR has smaller leak conductance compared to Wistar rats (Moraes et al., 2014). Here, we extend the model to incorporate similar change in the pre-I/I population to explain CIH induced plasticity to the respiratory CPG. Increased excitability of pre-I/I population readily explains a lower apneic threshold after CIH. By adding a glutamatergic excitatory projection from this pre-I/I population to the late-E population in the pFRG, the increased excitability in the pre-BötC is integrated by the pFRG to lower its threshold for activation. This projection mediates a change in the active expiration threshold induced by plasticity to the pre-I/I population in the CIH model.

In the model, we incrementally increased central chemosensory drive in the control and CIH models to simulate progressive increase in blood CO_2 from normocapnia at 5% to mild and then strong hypercapnia at respectively 7% and 10% partial pressure of CO_2 (Fig. 9A). To accommodate progressive hypercapnia in the model, we changed the weight of the CO_2 sensitive drive to RTN-cpg and RTN-late-E to 1.2 nS for 7% CO_2 and to 1.32 nS for 10% CO_2. This simulation is parallel to experiments performed in the arterially perfused preparation where the partial pressure of CO_2 in the perfusate was implemented over the same incremental range (Molkov et al., 2011) (Fig. 1). In the control model, active expiration (marked by the presence of late-E activity in the AbN)

emerges at 7% CO_2 (Fig. 9A). The frequency of these late-E AbN bursts increased in a quantal fashion (Molkov et al., 2010, Rubin et al., 2011) from 1:2 AbN bursts per inspiratory PN bursts at 7% CO_2 to 1:1 AbN bursts per inspiratory PN bursts at 10% CO_2. In the CIH model, the threshold for emergence of late-E AbN activity is decreased (Fig. 9A) as in normocapnia (5% partial pressure of CO_2), AbN bursts are already present after CIH conditioning.

We incrementally decreased central chemosensory drive in the control and CIH models to simulate a progressive decrease in blood CO_2 partial pressure from normocapnia at 5% blood CO_2 to mild and then strong hypocapnia - 3% and 1% partial pressure of CO_2 respectively. We accomplished progressive hypocapnia in the model by decreasing the weight of the CO_2 sensitive drive to RTN-cpg and RTN-late-E to 0.72 nS for 3% CO_2 and to 0 nS for 1% CO_2. In the control model, respiratory activity—represented as inspiratory bursts reflected in the PN—persists in mild hypocapnia (Fig. 9B, Control, 3% CO_2) but disappears in strong hypocapnia (Fig. 9B, Control, 1% CO_2). After CIH a decrease from 5% to 3% CO_2 eliminates late-E discharges in AbN (Fig. 9B, After CIH). A further decrease to 1% CO_2 does not stop the respiratory rhythm as opposed to the control case, which is similar to findings in the rat (Reference).

Discussion

The model presented qualitatively reproduced the effects of peripheral chemoreflex activation in the arterially perfused preparation of decerebrate rats. By changing a subset of biophysical parameters, the model was also able to reproduce the response to progressive hypercapnia and hypocapnia as well as increased sympathoexcitation in CIH. This model provided possible mechanistic explanations to the peripheral chemoreflex response and to plasticity induced by CIH. The model was based on several hypotheses that can be tested in experimental animals (each developed further below): (Hypothesis 1) 2^{nd}-order peripheral chemoreceptive neurons in the NTS project directly to the RTN central chemoreceptors (the anatomical projections were previously confirmed by Takakura et al. (2006)); (Hypothesis 2) sympathetic neurons in the RVLM receive convergent excitatory inputs from late-E (pFRG), a post-I population

in the cVRG, and 2nd-order chemoreceptive neurons in the NTS; and (Hypothesis 3) CIH-induced plasticity in the brainstem circuits can be explained be a down-regulation of ohmic leak channels in the pre-I/I population (pre-BötC).

Peripheral chemoreflex in control rats

During peripheral chemoreceptor stimulation the respiratory frequency substantially increases (Fig. 2) whereas RTN central chemoreceptor activation during hypercapnia does not lead to significant frequency variations (Molkov et al., 2010, Molkov et al., 2014a). Based on this we assumed that NTS peripheral chemoreceptors accelerate phrenic discharges by exciting the inspiratory neurons in the pre-BotC which was reflected in the model by direct excitatory projections from NTS to the pre-I/I population (Fig. 4). This possibility is supported by previous studies showing that microinjections of glutamate in the pre-BötC increase PN frequency *in vivo* and *in situ* while the antagonism of ionotropic glutamatergic receptors in this area eliminated the PN, but not the AbN and tSN responses to peripheral chemoreflex activation *in situ* (Moraes et al., 2011, Moraes et al., 2012c).

Peripheral chemoreceptor activation led to the emergence of late-E discharges in the abdominal and sympathetic nerve activities (Fig. 2). These late-E bursts strongly resembled the discharges appearing in the same nerves during hypercapnia (Molkov et al., 2011). Appearance of late-E activity during hypercapnia is mediated by the increased tonic drive provided by the RTN chemoreceptors (Molkov et al., 2010). Further, late-E discharges emerging in AbN and tSN during peripheral chemoreceptor stimulation can be abolished by pharmacological suppression of the RTN (Moraes et al., 2012a). These facts are consistent with the hypothesis that NTS second order peripheral chemoreceptive neurons send excitatory inputs to the RTN central chemoreceptors (Takakura et al., 2006) (**Hypothesis 1**). This was implemented in the model as direct excitatory projections from 2nd order peripheral chemoreceptive NTS neurons to RTN chemoreceptors (Fig. 4).

Activation of peripheral chemoreceptors was accompanied by powerful discharges in HN, cVN, AbN, and tSN motor outputs during the post-inspiratory phase of the respiratory cycle (Fig. 2). This means that activation of 2nd order NTS

chemoreceptive cells may have a direct excitatory effect on expiratory neurons. Direct excitation of post-I or aug-E neurons in the BötC compartment of the respiratory CPG would be inconsistent with an increase in the respiratory frequency. Accordingly, we suggest that this post-I activity is recruited at the level of pattern formation rather than pattern generation. In the model, we placed a new population in the cVRG which is silent at baseline conditions.

There is well-documented evidence of direct excitatory projections from 2nd order NTS peripheral chemoreceptive neurons to the RVLM (see Accorsi-Mendonca and Machado (2013) for review) which mediate sympathoexcitatory effect of peripheral chemoreceptor stimulation. Our model implies that there are at least two more indirect pathways mediated by the respiratory neurons (**Hypothesis 2**).

The first is a consequence of excitatory projections from RTN late-E population to RVLM suggested in our previous publications (Baekey et al., 2010, Molkov et al., 2011, Rybak et al., 2012, Molkov et al., 2014b) to explain appearance of late-E discharges in the sympathetic activity during hypercapnia. The RTN late-E population receives excitatory drive from the RTN central chemoreceptors which increases with blood CO_2 level due to their intrinsic CO_2 chemosensitivity. Our model suggests that an excitatory input from the NTS peripheral chemoreceptors to RTN central chemoreceptors (Takakura et al., 2006), is functionally important to activate RTN late-E neurons and to consequently evoke late-E discharges in the sympathetic nerve during peripheral chemoreceptor stimulation. The critical role of the RTN in the generation of late-E bursts during peripheral chemoreflex was previously demonstrated (Moraes et al., 2012a).

The second indirect pathway is mediated by the post-I population, which we introduced to explain the occurrence of strong post-inspiratory discharges in multiple respiratory and sympathetic motor outputs, and putatively placed to the cVRG compartment of the respiratory network. This new population receives inhibition during inspiratory and E2 phases, and can only activate during post-inspiration by an excitatory peripheral chemoreceptor drive from NTS. Apparently, this post-I mediated pathway seems to play a dominant role, since the depression of post-I activity elicited either by the glutamatergic antagonism in the NTS (Costa-Silva et al., 2010) or pontine-medullary

585 transection (Baekey et al., 2008) significantly attenuated the sympatho-excitatory
586 response to peripheral chemoreflex stimulation.
587
588 ***CIH-induced central and peripheral plasticity***
589
590 Given that the pre-I/I population of the pre-BötC is a primary target for tonic
591 excitatory drives to the respiratory CPG and that these drives are strongly activated
592 during the peripheral chemoreflex response (Moraes et al., 2014), we speculated that
593 repetitive activation of the peripheral chemoreflex may induce plasticity of channel
594 expression due to prolonged excessive excitation. Recent evidence in SHR indicates a
595 decrease in the leak conductance of pre-inspiratory neurons in the pre-Bötzinger complex
596 (Moraes et al., 2014) which elevates their excitability. Our model shows that similar
597 changes as a result of CIH exposure may explain abovementioned downshifts in the CO_2
598 thresholds (**Hypothesis 3**). However, the mechanisms responsible for such plasticity
599 remains to be found.
600 One possibility is that this change is mediated by downregulation of potassium
601 leak channels. Persistent and repetitive activation of group I metabotrobic glutamate
602 receptors over the course of CIH conditioning would increase the catalyzation of
603 diacylglycerol, leading to activation of protein kinase C and the subsequent decrease of
604 the leak conductance through channel protein trafficking (Gabriel et al., 2012). Another
605 example of similar changes consistent with the timescale considered in our study is an
606 excitotoxicity-mediated transcriptional decrease in HCN channel function found to
607 increase excitability of CA1 cells (Adams et al., 2009). In that study an induced increase
608 in synchronous burst duration correlated with a reduction in HCN2 mRNA levels which
609 persisted for at least 7 days. HCN channels are primarily permeable to K^+ ions, and,
610 hence, their downregulation positively affects the excitability. This is consistent with the
611 recent idea of peripheral chemoreceptor mediated channelopathy within the respiratory
612 network in SHRs (Moraes et al., 2015).
613 As already mentioned, after CIH conditioning the respiratory CPG exhibits higher
614 respiratory rate and lower CO_2 thresholds for both late-E activity emergence and
615 hypocapnic apnea (Figs. 1, 9). Previously this was explained by increased CO_2 sensitivity

of the RTN central chemoreceptors following CIH exposure (Molkov et al., 2011) but no experimental evidence of any intrinsic changes in the central chemoreceptors is available. Our present model provides a different explanation based on increased excitability of the pre-BötC pre-I/I population discussed above. Since this population is a main driver of the inspiratory activity in the network, its increased excitability alone would lead to a lesser dependence on excitatory drive from RTN central chemoreceptors and, hence, to a lower apneic threshold. To explain the lower threshold for late-E emergence, we hypothesize and implement in the model that pre-I/I neurons send excitatory projections to the RTN late-E population (Fig. 4). Due to increased excitability after CIH exposure, pre-I/I neurons increase their firing including the pre-I (late-E) phase and thus provide additional excitation to the RTN late-E population which underlies the emergence of late-E activity at lower CO_2 levels (Fig. 9).

CIH conditioned rats exhibit a stronger peripheral chemoreflex evoked sympathetic response than control animals (Fig. 3). We speculated that this effect reflects stronger activation of the direct sympathoexcitatory pathway rather than indirect inputs from respiratory populations. This assumption is in accord with the fact that CIH exposure increases the duration but not the magnitude of the respiratory response to peripheral chemoreceptor stimulation (Fig. 3). We suggest that the underlying mechanism is chronic sensitization of peripheral chemoreceptors during CIH conditioning which finds strong experimental support (Abdala et al2012; Pawar et al., 2008, Tan et al., 2010, Zoccal et al., 2011, Costa-Silva et al., 2012, Kumar and Prabhakar, 2012). That is not to say that baseline facilitation of motoneuron activity in CIH rats is dependent on peripheral chemoreceptor sensitization. For example, AbN and tSN late-E activity persists despite carotid body transection after CIH conditioning (Zoccal et al., 2008).

Alternative brainstem plasticity could contribute to increased peripheral chemoreflex sympathoexcitation after CIH conditioning. For example glutamatergic transmission in the NTS is augmented in CIH (Costa-Silva et al., 2012). In this case, plasticity of NTS chemoreceptive neural response to peripheral chemoreflex stimulation could amplify the motoneuron responses independent of the strength of the input from the carotid body. Besides, CIH conditioning increases the strength of the purinergic sympathoexcitatory response in the RVLM (Zoccal et al., 2011). This mechanism could

account for increased sympathoexcitatory response to peripheral chemoreflex stimulation. In the model we implement that as a greater activity of the 2nd-order chemoreceptive NTS neurons in CIH-conditioned animals as compared to the naïve ones. Our simulations support the plausibility of this assumption (Fig. 8).

Summary and Conclusions

The generation of novel bursts in sympathetic activity coupled with the emergence of active expiration has been highlighted as an important mechanism underpinning high levels of sympathetic activity and arterial pressure in rats submitted to CIH (Zoccal et al., 2008, Zoccal et al., 2009, Moraes et al., 2013). Although carotid body chemoreceptors were found to be critical for the development of CIH-induced arterial hypertension (Fletcher et al., 1992), inputs from peripheral chemoreceptors are not required for the maintenance of expiratory component of the sympathetic activity – since the carotid body removal after CIH exposure did not eliminate late-E activity in the sympathetic nerve (Molkov et al., 2011). In fact, hypocapnia-induced reduction of respiratory drive canceled the sympathetic and abdominal late-E bursts in CIH rats and rescued the normal sympathetic burst pattern (Molkov et al., 2011), indicating that coupling between respiratory and sympathetic networks is a critical mechanisms for maintenance of sympathetic overactivity after CIH exposure. In our study, we sought to identify the potential neural mechanisms required for the development of active expiration and sympathetic overactivity in CIH rats.

In order to simulate motoneuron activity of rats conditioned by CIH, a subset of parameters in the CIH model were altered from the values in the control model. These changes reflected central and peripheral plasticity. We modeled central plasticity in the brainstem by increasing the excitability of the pre-I/I population. The conductance of the leak current in neurons of the pre-I/I population was changed from 2.9 nS to 2.3 nS. This change mediated the hypocapnic shift in apneic threshold and the threshold for the emergence of active expiration (Fig. 9). We mimicked peripheral plasticity due to CIH by increasing the excitatory drive to 2nd-order chemoreceptive neurons in the NTS during peripheral chemoreflex. In the control model, the weight of this drive was 0.75 nS, and it

678 increased in magnitude to 1.6 nS in the CIH model. The effect of this change is only
679 visible during stimulation of the peripheral chemoreflex (Fig. 8).
680 Our hypothesis implies that the discussed plastic changes in the respiratory
681 network critically depend on the peripheral chemoreceptor input and not on hypoxia per
682 se. This is indirectly supported by multiple experimental studies (see (Paton et al., 2013a)
683 for review) and emphasizes the importance of carotid bodies as a possible therapeutic
684 target for treating neurogenic hypertension (McBryde et al. 2013; Paton et al., 2013b).
685

686 # Acknowledgements

687

688 This study was supported by NIH grant #R01 AT008632 to YIM, APL and DZ. IAR is
689 funded by NIH grant #R01 NS069220. DZ is funded by São Paulo State Foundation
690 (FAPESP, grant # 2013/17251-6). JFRP is funded by the British Heart Foundation. APL
691 is funded by the International Rett Syndrome Foundation. This work utilized the
692 computational resources of the NIH HPC Biowulf cluster. (http://hpc.nih.gov).
693

694 # Figure legends

695

696 **Figure 1**. Recordings depict activity of PN and AbN under progressive hypocapnia and
697 hypercapnia in in situ preparations of control and CIH rats. The hypercapnic threshold for
698 emergence of late-expiratory activity in AbN decreases after CIH. The hypocapnic
699 threshold for the appearance of respiratory activity in PN is also decreased in CIH rats.
700 Adapted from (Molkov et al., 2011).
701

702 **Figure 2**. Appearance of additional motoneuron activation during peripheral
703 chemoreceptor activation. Tracings from two recordings from *in situ* preparations (panels
704 **A** and **B**), representative from the group, showing the changes in the HN, cVN, PN, AbN
705 and tSN in response to peripheral chemoreceptor activation by KCN (arrows, 0.05%).
706 Note that during chemoreflex activation, post inspiratory activity increases in cVN and
707 novel post-inspiratory components appears in tSN, AbN, and HN. Late expiratory activity

also appears in SN, AbN, and HN. Gray bars highlight post-inspiratory phases of the respiratory cycle. **C**. Percent changes in amplitude of different motor outputs during peripheral chemoreflex activation.

Figure 3. CIH exaggerates respiratory and sympathetic chemoreflex responses. **A**. Tracings from control (left) and CIH (right) rats, representative from their respective experimental group, showing the PN and tSN responses to stimulation of the peripheral chemoreflex with KCN (arrows). Note the amplified tSN response during peripheral chemoreceptor stimulation in CIH rats. B. Tracings from control (left) and CIH (right) rats, representative from their respective experimental group, showing the PN and AbN responses to stimulation of the peripheral chemoreflex with KCN (arrows). Note the prolonged AbN response during peripheral chemoreceptor stimulation in CIH rats. **C**. Percent change in tSN amplitude during peripheral chemoreflex in control and CIH rats. * denotes statistically significant difference. See text for details. **D**. Time course of the percent change in respiratory frequency relative to baseline after peripheral chemoreceptor activation with KCN for control (open squares) and CIH (filled squares) groups. Data are shown as mean±SD. Note prolonged frequency response in CIH group. **E**. No significant difference in percent change in AbN amplitude during peripheral chemoreflex between control and CIH groups. **F**. Durations of post-I and late-E expiratory phases relative to the expiration duration in control and CIH groups during peripheral chemoreflex. **G**. No significant difference in percent change in cVN amplitude during peripheral chemoreflex between control and CIH groups.

Figure 4. Network connectivity diagram for model of brainstem respiratory circuits. Brainstem compartments: VRC, ventral respiratory column; BötC, Bötzinger complex; pre-Bötzinger complex; rVRG, rostral ventral respiratory group; cVRG, caudal ventral respiratory group; NTS, nucleus tractus solitarii; RTN/pFRG retrotrapezoid nucleus/parafacial respiratory group; RVLM, rostral ventrolateral medulla; CVLM, caudal ventrolateral medulla. Neural populations: pre-I/I, pre-inspiratory/inspiratory; early-I(1), early inspiratory (1); ramp-I, ramp inspiratory; early-I(2), early inspiratory (2); post-I, post inspiratory; post-I (e), post inspiratory excitatory; aug-E, augmenting

739 expiratory; 2nd Chemo, 2nd-order chemoreceptors; bulbo-spinal post-I, bulbo-spinal post
740 inspiratory; late-E, late expiratory; IE, inspiratory-expiratory phase-spanning; RTN-CPG,
741 CO2-sensitive population projecting to CPG and late-E (pFRG); RTN-late-E, CO2-
742 sensitive population projecting just to late-E (pFRG). Motoneurones: PN, phrenic nerve;
743 AbN, abdominal nerve; tSN, thoracic sympathetic nerve; HN, hypoglossal nerve; cVN,
744 cervical vagus nerve. Excitatory neural populations, inhibitory neural populations, and
745 excitatory drives are respectively represented as orange spheres, blue spheres, and green
746 triangles. Motoneurones are depicted as brown spheres. Red projections originating in
747 neural populations depict excitatory projections. Blue projections originating in neural
748 populations depict inhibitory projections. Green projections indicate the distribution of
749 excitatory tonic drive. The bold excitatory pathways emphasize converging peripheral
750 chemosensitive projections to the pre-I/I population. Populations that were not included
751 in a previous model are marked with an asterisk.
752
753 **Figure 5**. Simulation depicting the response of motoneuron output (HN, cVN, PN, AbN,
754 and tSN) to the activation of the peripheral chemoreflex (**A**) and the motoneuron
755 response during suppression of RTN (**B**). (**A**) During activation of peripheral
756 chemoreflex, network frequency increases; post-inspiratory activity appears in HN, AbN,
757 and tSN motor nerves, and post-inspiratory activity in cVN increases in amplitude. Late
758 expiratory activity appears in HN, AbN, and tSN. (**B**) The suppression of the RTN
759 abolishes late-expiratory activity in HN, AbN, and tSN but has little effect on post-I
760 activity. The interval highlighted in yellow corresponds to the duration over which the
761 peripheral chemoreflex is stimulated. Baseline activity of PN is highlighted in grey to
762 emphasize the difference in frequency in the control model and the model with RTN
763 suppressed before the peripheral chemoreflex stimulation.
764
765 **Figure 6**. Simulation of activity of respiratory and sympathetic populations (early-I (1)
766 (pre-BötC), post-I (BötC), aug-E (BötC), late-E (pFRG), and post-I (cVRG)) before and
767 during stimulation of peripheral chemoreflex (**A**) and the activity of respiratory and
768 sympathetic populations under suppression of RTN during stimulation of peripheral
769 chemoreflex (**B**). (**A**) Peripheral chemoreflex increases drive to the respiratory central

pattern generator—increases network frequency and activating the late-E (pFRG) and post-I(cVRG) populations. (**B**) The suppression of RTN for the duration of the simulation abolishes expiratory activity in the late-E (pFRG) population.

Figure 7. Blow-up of activity during peripheral chemoreflex in the control model. Motoneuron output is compared to the activity of late-E (pFRG) and post-I (cVRG). Activity during late-E and post-I phases are highlighted in yellow and grey, respectively.

Figure 8. Simulations of (**A**) the control model and (**B**) the CIH model depicting activity in PN and tSN. The amplitude of tSN activity is increased in the CIH model compared to the control model with late-E bursting present.

Figure 9. Simulations of progressive (**A**) hypercapnia and (**B**) hypocapnia in PN and AbN in the control model and the CIH model. (**A**) Simulations reproduce hypocapnic shift in threshold for the emergence of late-expiratory activity in the AbN in the CIH model. (**B**) Simulations reproduce hypocapnic shift in the onset of respiratory activity of the PN in the CIH model.

References

Abdala AP, McBryde FD, Marina N, Hendy EB, Engelman ZJ, Fudim M, Sobotka PA, Gourine AV, Paton JF (2012) Hypertension is critically dependent on the carotid body input in the spontaneously hypertensive rat. J Physiol 590:4269-4277.

Abdala AP, Rybak IA, Smith JC, Paton JF (2009) Abdominal expiratory activity in the rat brainstem-spinal cord in situ: patterns, origins and implications for respiratory rhythm generation. J Physiol 587:3539-3559.

Accorsi-Mendonca D, Machado BH (2013) Synaptic transmission of baro- and chemoreceptors afferents in the NTS second order neurons. Autonomic neuroscience : basic & clinical 175:3-8.

799 Adams BE, Reid CA, Myers D, Ng C, Powell K, Phillips AM, Zheng T, O'Brien TJ,
800 Williams DA (2009) Excitotoxic-mediated transcriptional decreases in HCN2
801 channel function increase network excitability in CA1. Exp Neurol 219:249-257.
802 Aicher SA, Saravay RH, Cravo S, Jeske I, Morrison SF, Reis DJ, Milner TA (1996)
803 Monosynaptic projections from the nucleus tractus solitarii to C1 adrenergic
804 neurons in the rostral ventrolateral medulla: comparison with input from the
805 caudal ventrolateral medulla. J Comp Neurol 373:62-75.
806 Baekey DM, Dick TE, Paton JF (2008) Pontomedullary transection attenuates central
807 respiratory modulation of sympathetic discharge, heart rate and the baroreceptor
808 reflex in the in situ rat preparation. Exp Physiol 93:803-816.
809 Baekey DM, Molkov YI, Paton JF, Rybak IA, Dick TE (2010) Effect of baroreceptor
810 stimulation on the respiratory pattern: insights into respiratory-sympathetic
811 interactions. Respir Physiol Neurobiol 174:135-145.
812 Braga VA, Soriano RN, Machado BH (2006) Sympathoexcitatory response to peripheral
813 chemoreflex activation is enhanced in juvenile rats exposed to chronic
814 intermittent hypoxia. Exp Physiol 91:1025-1031.
815 Briant LJ, O'Callaghan EL, Champneys AR, Paton JF (2015) Respiratory modulated
816 sympathetic activity: A putative mechanism for developing vascular resistance? J
817 Physiol.
818 Caples SM, Gami AS, Somers VK (2005) Obstructive sleep apnea. Ann Intern Med
819 142:187-197.
820 Carey RM (2013) Resistant hypertension. Hypertension 61:746-750.
821 Costa-Silva JH, Zoccal DB, Machado BH (2010) Glutamatergic antagonism in the NTS
822 decreases post-inspiratory drive and changes phrenic and sympathetic coupling
823 during chemoreflex activation. J Neurophysiol 103:2095-2106.
824 Costa-Silva JH, Zoccal DB, Machado BH (2012) Chronic intermittent hypoxia alters
825 glutamatergic control of sympathetic and respiratory activities in the commissural
826 NTS of rats. Am J Physiol Regul Integr Comp Physiol 302:R785-793.
827 Dick TE, Hsieh YH, Morrison S, Coles SK, Prabhakar N (2004) Entrainment pattern
828 between sympathetic and phrenic nerve activities in the Sprague-Dawley rat:

829 hypoxia-evoked sympathetic activity during expiration. Am J Physiol Regul
830 Integr Comp Physiol 286:R1121-1128.
831 Dudenbostel T, Calhoun DA (2011) Resistant hypertension, obstructive sleep apnoea and
832 aldosterone. Journal of human hypertension.
833 Esler M (2009) The 2009 Carl Ludwig Lecture: pathophysiology of the human
834 sympathetic nervous system in cardiovascular diseases: the transition from
835 mechanisms to medical management. J Appl Physiol 108:227-237.
836 Fisher JP, Paton JF (2012) The sympathetic nervous system and blood pressure in
837 humans: implications for hypertension. J Hum Hypertens 26:463-475.
838 Fletcher EC (2001) Invited review: Physiological consequences of intermittent hypoxia:
839 systemic blood pressure. J Appl Physiol 90:1600-1605.
840 Fletcher EC, Lesske J, Culman J, Miller CC, Unger T (1992) Sympathetic denervation
841 blocks blood pressure elevation in episodic hypoxia. Hypertension 20:612-619.
842 Gabriel L, Lvov A, Orthodoxou D, Rittenhouse AR, Kobertz WR, Melikian HE (2012)
843 The acid-sensitive, anesthetic-activated potassium leak channel, KCNK3, is
844 regulated by 14-3-3beta-dependent, protein kinase C (PKC)-mediated endocytic
845 trafficking. J Biol Chem 287:32354-32366.
846 Go AS, Mozaffarian D, Roger VL, Benjamin EJ, Berry JD, Blaha MJ, Dai S, Ford ES,
847 Fox CS, Franco S, Fullerton HJ, Gillespie C, Hailpern SM, Heit JA, Howard VJ,
848 Huffman MD, Judd SE, Kissela BM, Kittner SJ, Lackland DT, Lichtman JH,
849 Lisabeth LD, Mackey RH, Magid DJ, Marcus GM, Marelli A, Matchar DB,
850 McGuire DK, Mohler ER, 3rd, Moy CS, Mussolino ME, Neumar RW, Nichol G,
851 Pandey DK, Paynter NP, Reeves MJ, Sorlie PD, Stein J, Towfighi A, Turan TN,
852 Virani SS, Wong ND, Woo D, Turner MB, American Heart Association Statistics
853 C, Stroke Statistics S (2014) Executive summary: heart disease and stroke
854 statistics--2014 update: a report from the American Heart Association. Circulation
855 129:399-410.
856 Janczewski WA, Feldman JL (2006) Distinct rhythm generators for inspiration and
857 expiration in the juvenile rat. J Physiol-London 570:407-420.
858 Kearney PM, Whelton M, Reynolds K, Muntner P, Whelton PK, He J (2005) Global
859 burden of hypertension: analysis of worldwide data. Lancet 365:217-223.

860 Konecny T, Somers VK (2011) Vascular dysfunction in sleep apnea: not just a peripheral
861 concern. Hypertension 58:352-353.
862 Koshiya N, Guyenet PG (1996) Tonic sympathetic chemoreflex after blockade of
863 respiratory rhythmogenesis in the rat. J Physiol 491 (Pt 3):859-869.
864 Kumar P, Prabhakar NR (2012) Peripheral chemoreceptors: function and plasticity of the
865 carotid body. Compr Physiol 2:141-219.
866 Malpas SC (2010) Sympathetic nervous system overactivity and its role in the
867 development of cardiovascular disease. Physiol Rev 90:513-557.
868 McBryde FD, Abdala AP, Hendy EB, Pijacka W, Marvar P, Moraes DJ, Sobotka PA,
869 Paton JF (2013) The carotid body as a putative therapeutic target for the treatment
870 of neurogenic hypertension. Nature communications 4:2395.
871 Molkov YI, Abdala AP, Bacak BJ, Smith JC, Paton JF, Rybak IA (2010) Late-expiratory
872 activity: emergence and interactions with the respiratory CpG. J Neurophysiol
873 104:2713-2729.
874 Molkov YI, Shevtsova NA, Park C, Ben-Tal A, Smith JC, Rubin JE, Rybak IA (2014a) A
875 closed-loop model of the respiratory system: focus on hypercapnia and active
876 expiration. PloS one 9:e109894.
877 Molkov YI, Zoccal DB, Baekey DM, Abdala AP, Machado BH, Dick TE, Paton JF,
878 Rybak IA (2014b) Physiological and pathophysiological interactions between the
879 respiratory central pattern generator and the sympathetic nervous system. Prog
880 Brain Res 212:1-23.
881 Molkov YI, Zoccal DB, Moraes DJ, Paton JF, Machado BH, Rybak IA (2011)
882 Intermittent hypoxia-induced sensitization of central chemoreceptors contributes
883 to sympathetic nerve activity during late expiration in rats. J Neurophysiol
884 105:3080-3091.
885 Moraes DJ, Bonagamba LG, Zoccal DB, Machado BH (2011) Modulation of respiratory
886 responses to chemoreflex activation by L-glutamate and ATP in the rostral
887 ventrolateral medulla of awake rats. Am J Physiol Regul Integr Comp Physiol
888 300:R1476-1486.
889 Moraes DJ, da Silva MP, Bonagamba LG, Mecawi AS, Zoccal DB, Antunes-Rodrigues J,
890 Varanda WA, Machado BH (2013) Electrophysiological properties of rostral

ventrolateral medulla presympathetic neurons modulated by the respiratory network in rats. J Neurosci 33:19223-19237.

Moraes DJ, Dias MB, Cavalcanti-Kwiatkoski R, Machado BH, Zoccal DB (2012a) Contribution of the retrotrapezoid nucleus/parafacial respiratory region to the expiratory-sympathetic coupling in response to peripheral chemoreflex in rats. J Neurophysiol 108:882-890.

Moraes DJ, Machado BH, Paton JF (2014) Specific respiratory neuron types have increased excitability that drive presympathetic neurones in neurogenic hypertension. Hypertension 63:1309-1318.

Moraes DJ, Machado BH, Paton JF (2015) Carotid body overactivity induces respiratory neurone channelopathy contributing to neurogenic hypertension. J Physiol 593:3055-3063.

Moraes DJ, Zoccal DB, Machado BH (2012b) Medullary respiratory network drives sympathetic overactivity and hypertension in rats submitted to chronic intermittent hypoxia. Hypertension 60:1374-1380.

Moraes DJ, Zoccal DB, Machado BH (2012c) Sympathoexcitation during chemoreflex active expiration is mediated by L-glutamate in the RVLM/Botzinger complex of rats. J Neurophysiol 108:610-623.

Narkiewicz K, van de Borne PJ, Montano N, Dyken ME, Phillips BG, Somers VK (1998) Contribution of tonic chemoreflex activation to sympathetic activity and blood pressure in patients with obstructive sleep apnea. Circulation 97:943-945.

Paton JF (1996) A working heart-brainstem preparation of the mouse. J Neurosci Methods 65:63-68.

Paton JF, Ratcliffe L, Hering D, Wolf J, Sobotka PA, Narkiewicz K (2013a) Revelations about carotid body function through its pathological role in resistant hypertension. Curr Hypertens Rep 15:273-280.

Paton JF, Sobotka PA, Fudim M, Engleman ZJ, Hart EC, McBryde FD, Abdala AP, Marina N, Gourine AV, Lobo M, Patel N, Burchell A, Ratcliffe L, Nightingale A (2013b) The carotid body as a therapeutic target for the treatment of sympathetically mediated diseases. Hypertension 61:5-13.

921 Pawar A, Peng YJ, Jacono FJ, Prabhakar NR (2008) Comparative analysis of neonatal
922 and adult rat carotid body responses to chronic intermittent hypoxia. J Appl
923 Physiol (1985) 104:1287-1294.
924 Pedrosa RP, Drager LF, Gonzaga CC, Sousa MG, de Paula LK, Amaro AC, Amodeo C,
925 Bortolotto LA, Krieger EM, Bradley TD, Lorenzi-Filho G (2011) Obstructive
926 sleep apnea: the most common secondary cause of hypertension associated with
927 resistant hypertension. Hypertension 58:811-817.
928 Rubin JE, Bacak BJ, Molkov YI, Shevtsova NA, Smith JC, Rybak IA (2011) Interacting
929 oscillations in neural control of breathing: modeling and qualitative analysis. J
930 Comput Neurosci 30:607-632.
931 Rybak IA, Abdala AP, Markin SN, Paton JF, Smith JC (2007) Spatial organization and
932 state-dependent mechanisms for respiratory rhythm and pattern generation. Prog
933 Brain Res 165:201-220.
934 Rybak IA, Molkov YI, Paton JFR, Abdala APL, Zoccal DB (2012) Modeling the
935 Autonomic Nervous System. In: PRIMER ON THE AUTONOMIC NERVOUS
936 SYSTEM (Robertson, D. et al., eds): Elsevier Inc.
937 Simms AE, Paton JF, Pickering AE, Allen AM (2009) Amplified respiratory-sympathetic
938 coupling in the spontaneously hypertensive rat: does it contribute to hypertension?
939 J Physiol 587:597-610.
940 Smith JC, Abdala AP, Koizumi H, Rybak IA, Paton JF (2007) Spatial and functional
941 architecture of the mammalian brain stem respiratory network: a hierarchy of
942 three oscillatory mechanisms. J Neurophysiol 98:3370-3387.
943 Takakura AC, Moreira TS, Colombari E, West GH, Stornetta RL, Guyenet PG (2006)
944 Peripheral chemoreceptor inputs to retrotrapezoid nucleus (RTN) CO2-sensitive
945 neurons in rats. The Journal of physiology 572:503-523.
946 Tan ZY, Lu Y, Whiteis CA, Simms AE, Paton JF, Chapleau MW, Abboud FM (2010)
947 Chemoreceptor hypersensitivity, sympathetic excitation, and overexpression of
948 ASIC and TASK channels before the onset of hypertension in SHR. Circ Res
949 106:536-545.

Williams SK, Ravenell J, Jean-Louis G, Zizi F, Underberg JA, McFarlane SI, Ogedegbe G (2010) Resistant Hypertension and Sleep Apnea: Pathophysiologic Insights and Strategic Management. Curr Diab Rep.

Zoccal DB (2015) Peripheral chemoreceptors and cardiorespiratory coupling: a link to sympatho-excitation. Exp Physiol 100:143-148.

Zoccal DB, Bonagamba LG, Paton JF, Machado BH (2009) Sympathetic-mediated hypertension of awake juvenile rats submitted to chronic intermittent hypoxia is not linked to baroreflex dysfunction. Exp Physiol 94:972-983.

Zoccal DB, Bonagamba LGH, Oliveira FRT, Antunes-Rodrigues J, Machado BH (2007) Increased sympathetic activity in rats submitted to chronic intermittent hypoxia. Exp Physiol 92:79-85.

Zoccal DB, Huidobro-Toro JP, Machado BH (2011) Chronic intermittent hypoxia augments sympatho-excitatory response to ATP but not to L-glutamate in the RVLM of rats. Auton Neurosci 165:156-162.

Zoccal DB, Simms AE, Bonagamba LG, Braga VA, Pickering AE, Paton JF, Machado BH (2008) Increased sympathetic outflow in juvenile rats submitted to chronic intermittent hypoxia correlates with enhanced expiratory activity. J Physiol 586:3253-3265.

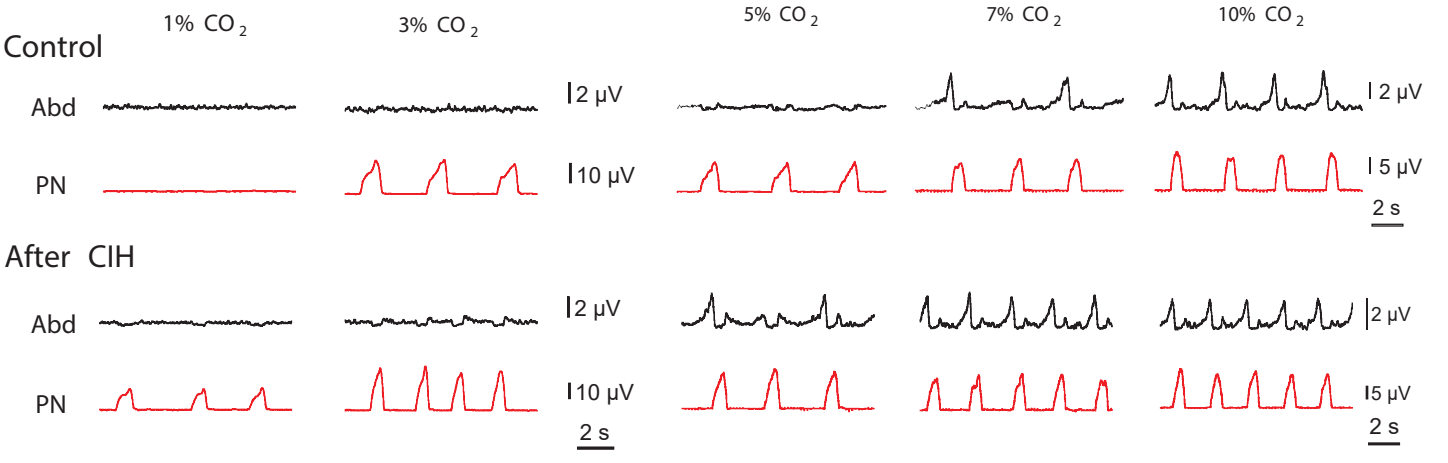
1% CO2
3% CO2
5% CO2
7% CO2
10% CO2
Control
Abd
PN
2 μV
10 μV
2 μV
5 μV
2 s
After CIH
Abd
PN
2 μV
10 μV
2 μV
5 μV
2 s
2 s

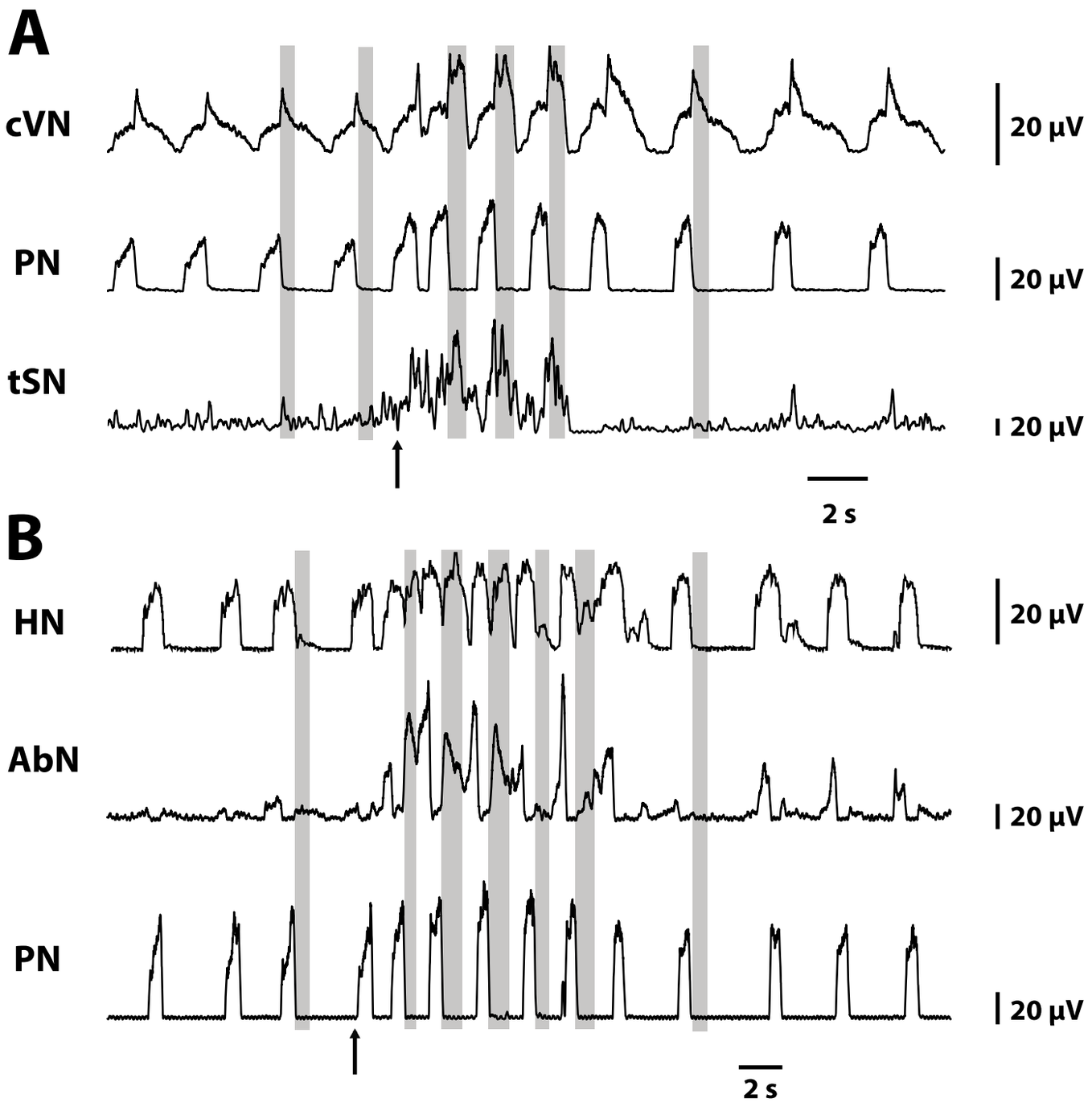
A
cVN
PN
tSN
20 µV
20 µV
20 µV
2 s
B
HN
AbN
PN
20 µV
20 µV
20 µV
2 s

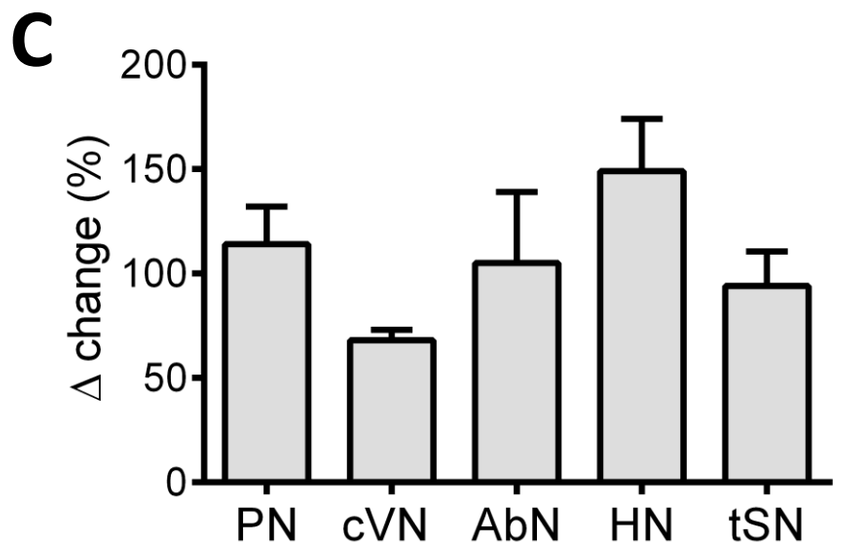
C
Δ change (%)
200
150
100
50
0
PN
cVN
AbN
HN
tSN

Figure 2

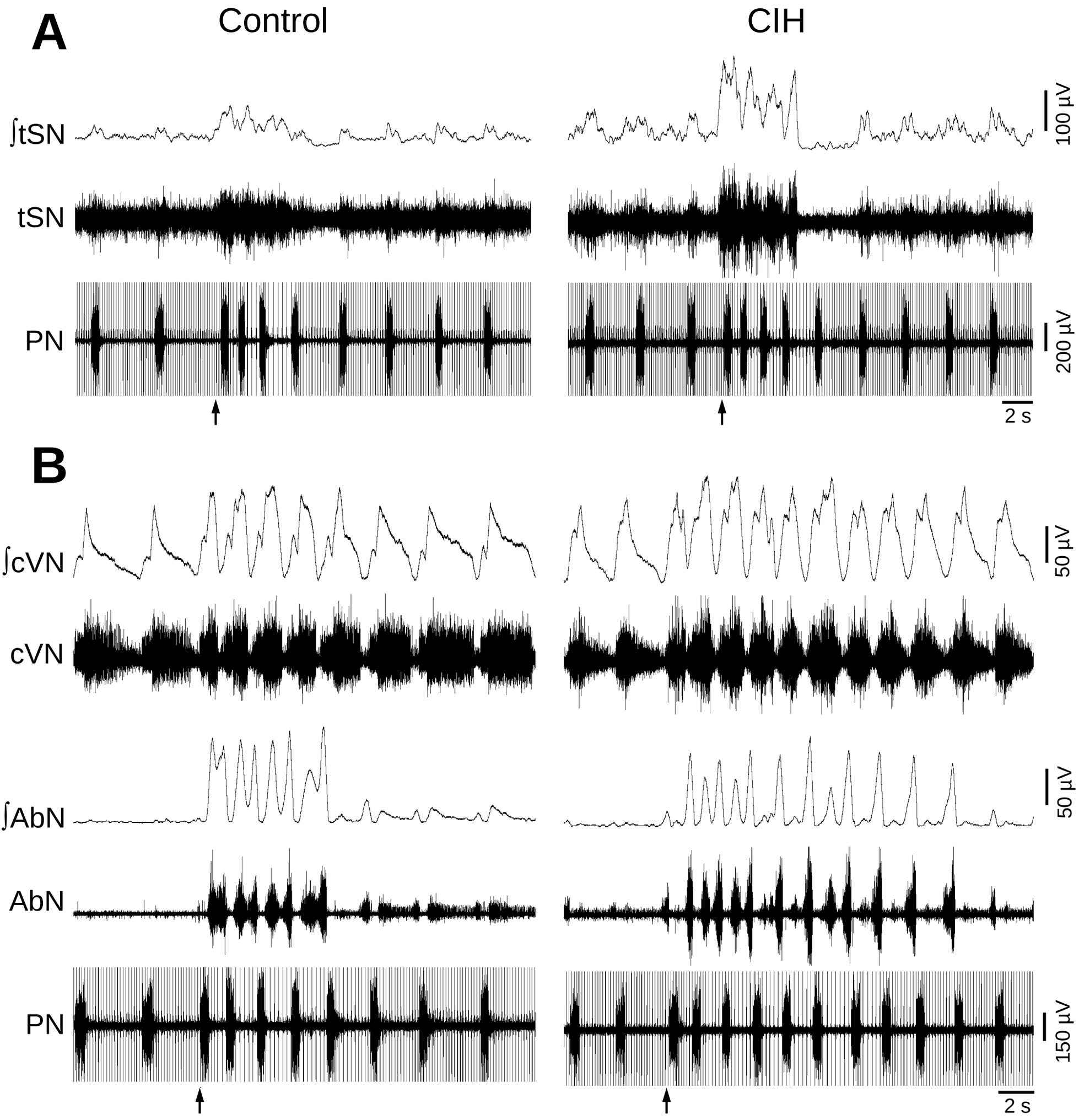
A
Control
CIH
∫tSN
tSN
PN
100 µV
200 µV
2 s
B
∫cVN
cVN
∫AbN
AbN
PN
50 µV
50 µV
150 µV
2 s

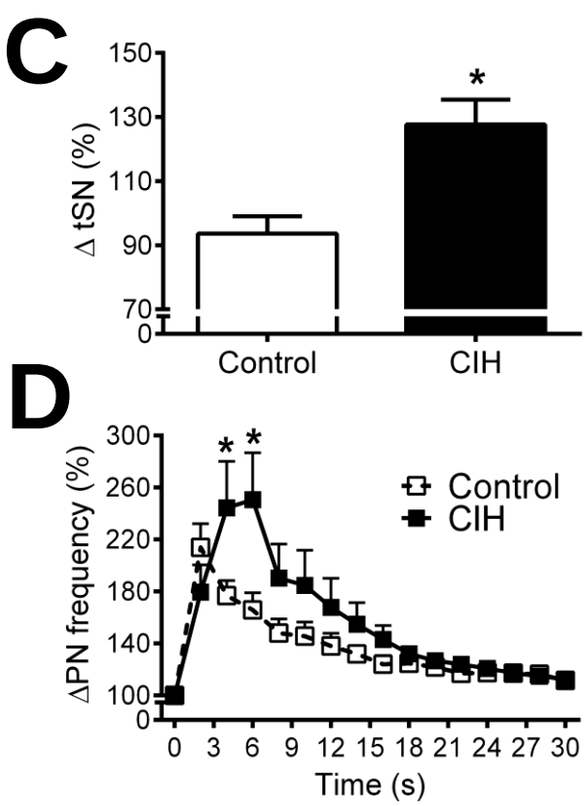
C
Δ tSN (%)
150
130
110
90
70
0
*
Control
CIH

D
ΔPN frequency (%)
300
260
220
180
140
100
0
* *
Control
CIH
0 3 6 9 12 15 18 21 24 27 30
Time (s)

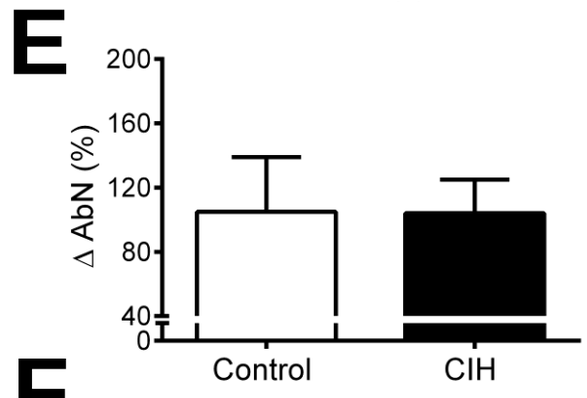
E
Δ AbN (%)
200
160
120
80
40
0
Control
CIH

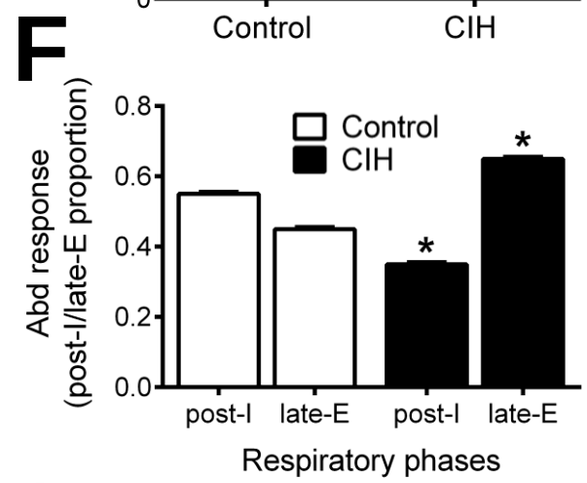
F
Abd response
(post-I/late-E proportion)
0.8
0.6
0.4
0.2
0.0
Control
CIH
*
*
post-I
late-E
post-I
late-E
Respiratory phases

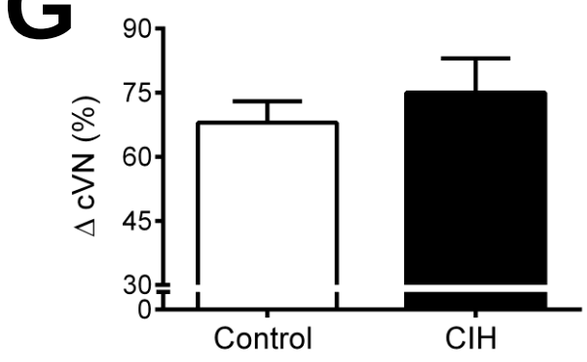
G
Δ cVN (%)
90
75
60
45
30
0
Control
CIH

Figure 3

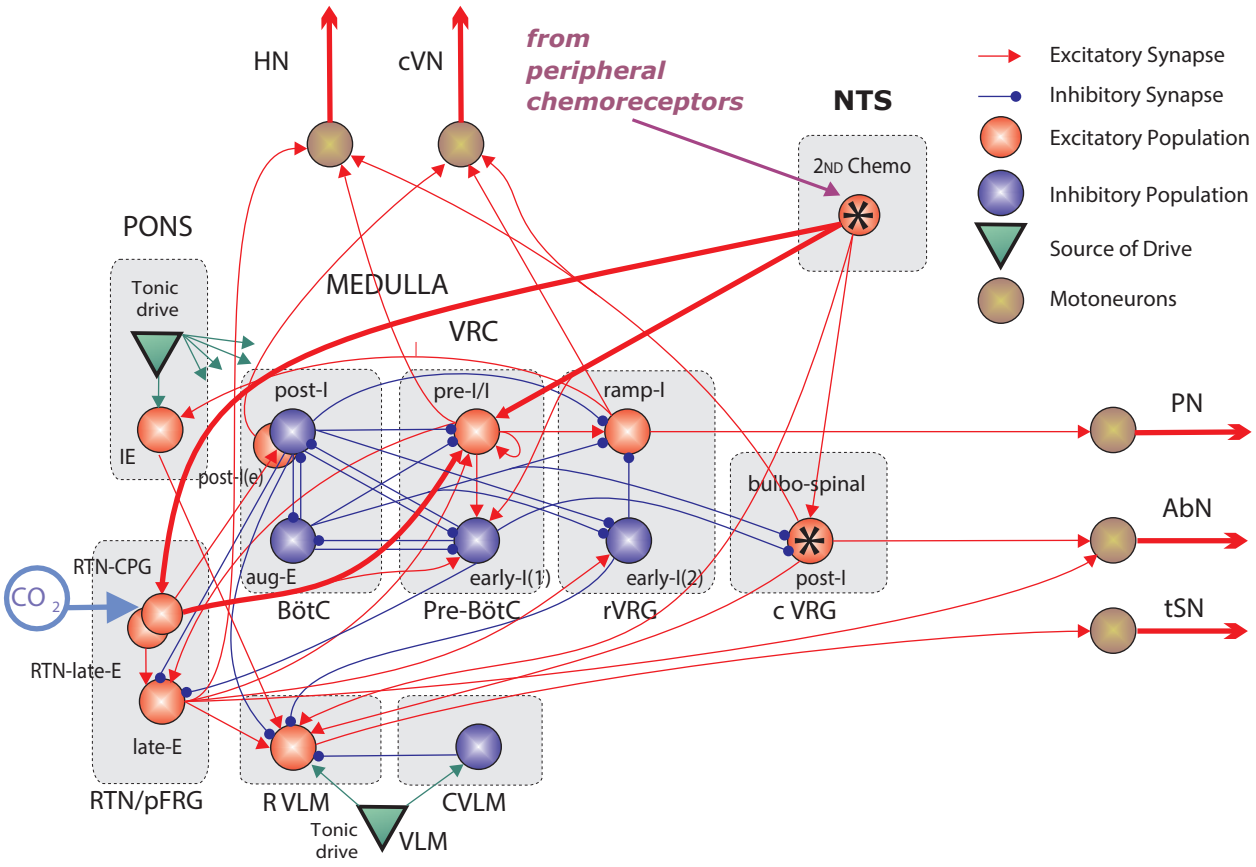
HN
cVN
from peripheral chemoreceptors
NTS
2ND Chemo
PONS
MEDULLA
VRC
Tonic drive
IE
post-I(e)
post-I
pre-I/I
ramp-I
aug-E
early-I(1)
early-I(2)
bulbo-spinal
post-I
BötC
Pre-BötC
rVRG
c VRG
RTN-CPG
CO2
RTN-late-E
late-E
RTN/pFRG
R VLM
CVLM
Tonic drive
VLM
PN
AbN
tSN
Excitatory Synapse
Inhibitory Synapse
Excitatory Population
Inhibitory Population
Source of Drive
Motoneurons

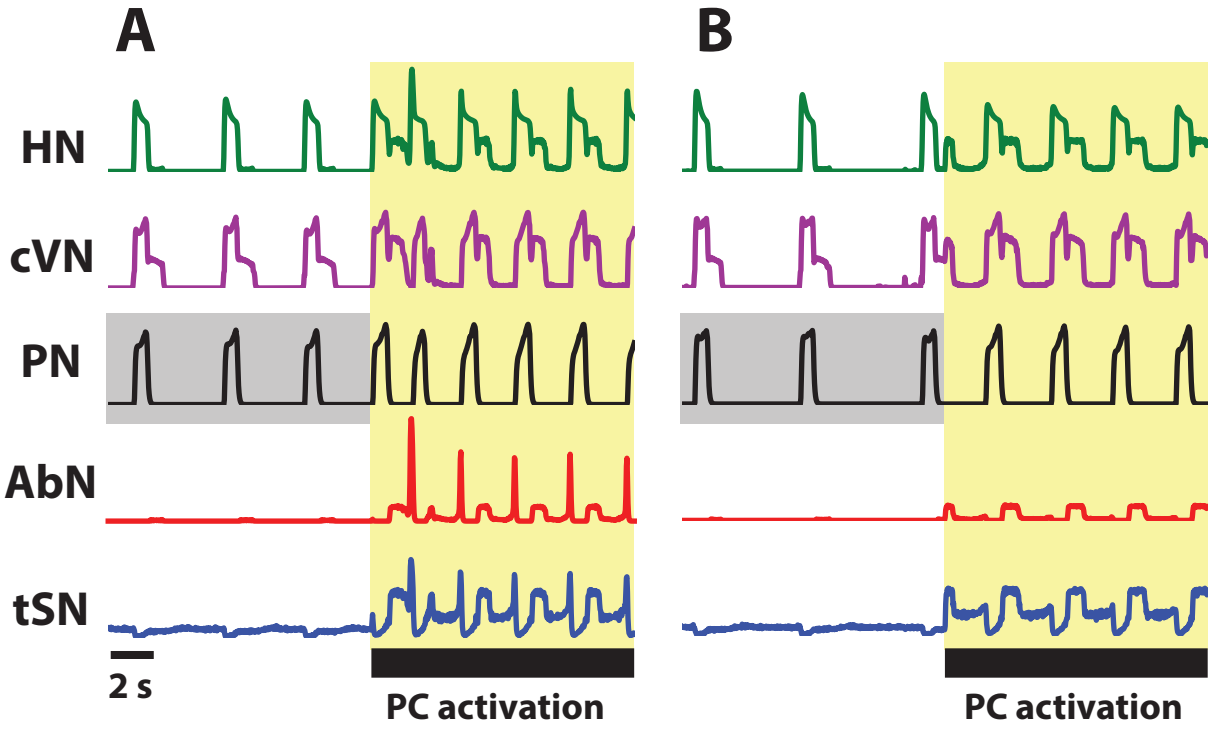
A
B
HN
cVN
PN
AbN
tSN
2 s
PC activation
PC activation

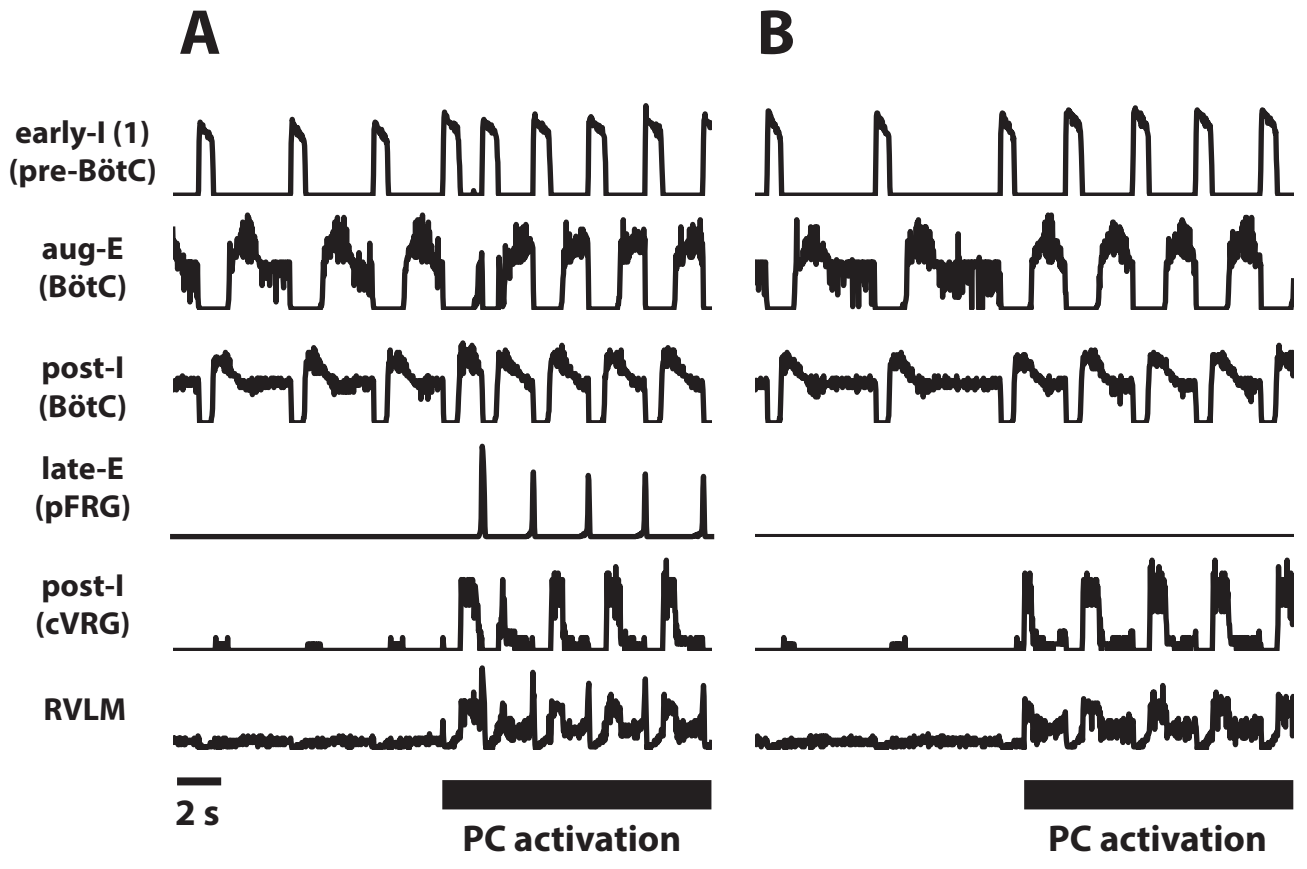
A
B
early-I (1)
(pre-BötC)
aug-E
(BötC)
post-I
(BötC)
late-E
(pFRG)
post-I
(cVRG)
RVLM
2 s
PC activation
PC activation

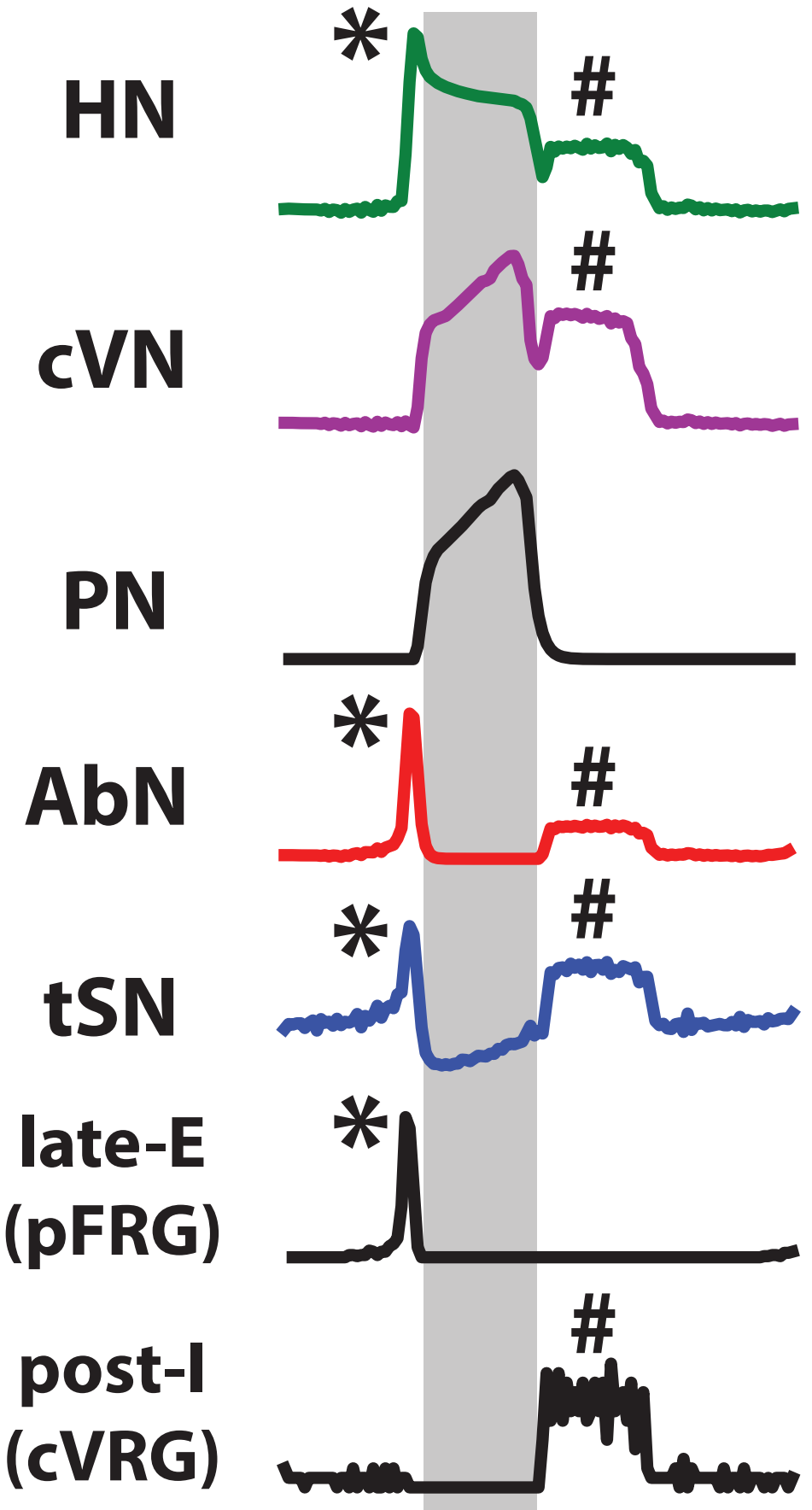
HN
cVN
PN
AbN
tSN
late-E
(pFRG)
post-I
(cVRG)
*
#

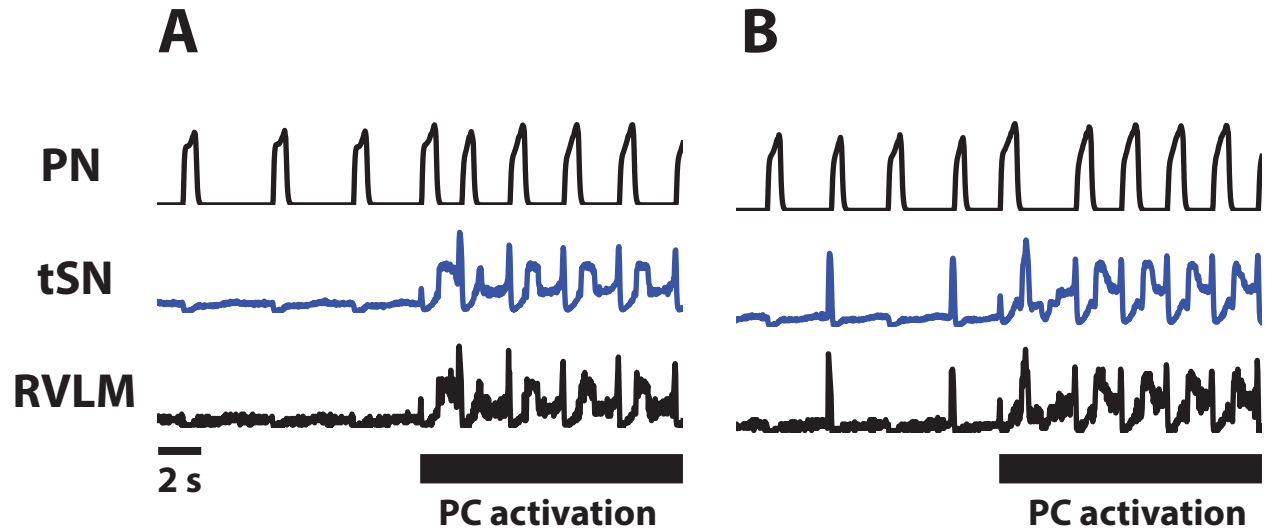
A
B
PN
tSN
RVLM
2 s
PC activation
PC activation

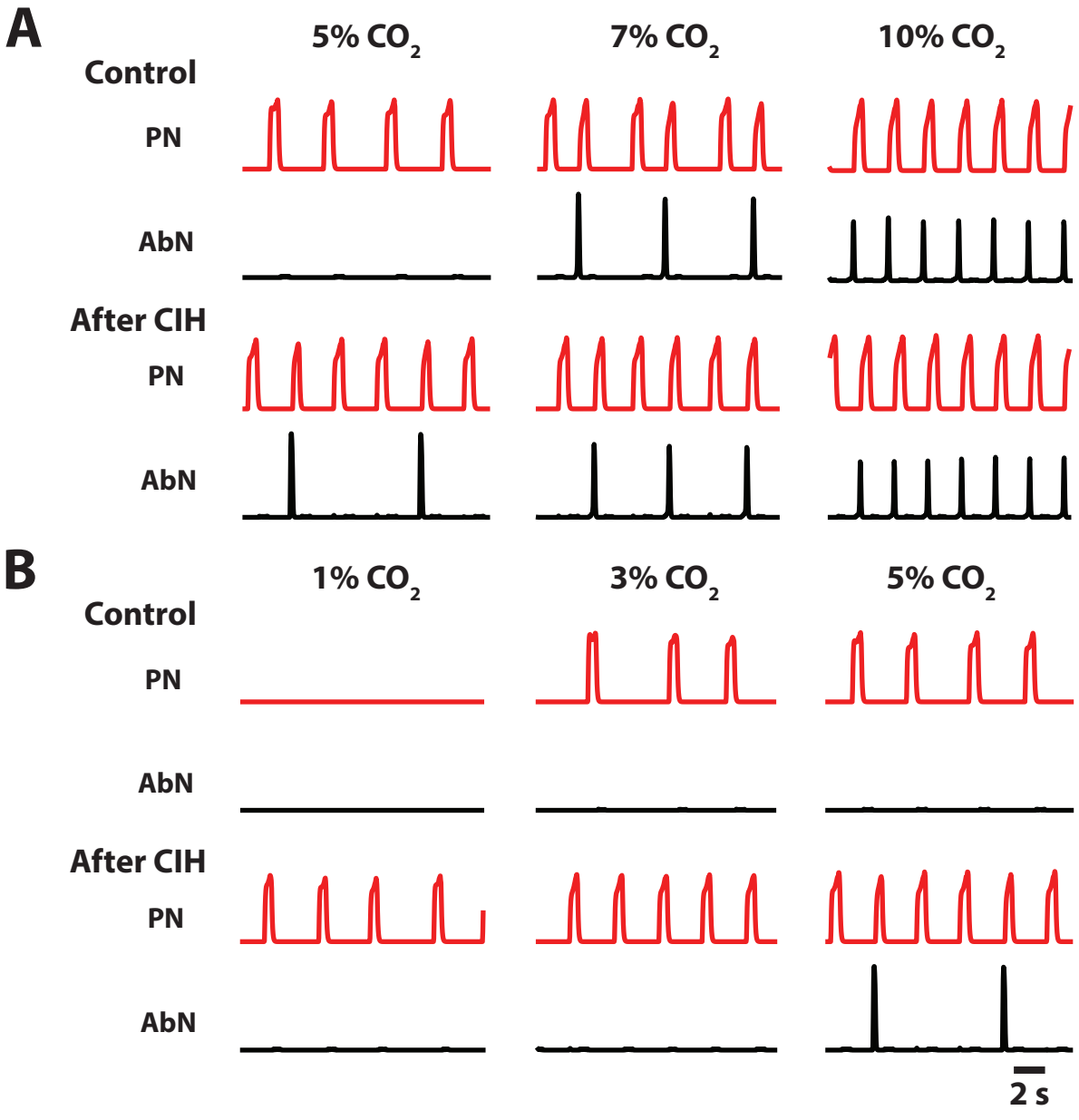
A
5% CO2
7% CO2
10% CO2
Control
PN
AbN
After CIH
PN
AbN
B
1% CO2
3% CO2
5% CO2
Control
PN
AbN
After CIH
PN
AbN
2 s